1 Introduction

Since 1967, the Nuclear Regulatory Commission (NRC) and its predecessor the Atomic Energy Commission (AEC) have conducted research programs that address aging of reactor components. The results of this research have been used to evaluate and establish regulatory guidelines to ensure acceptable levels of reliability for light water reactor (LWR) components. The products of this program, i.e., technical reports, methodologies for evaluating licensee submittals, and other inputs to the regulatory process, have led to the resolution of regulatory issues, as well as the development, validation, and improvement of regulations and regulatory guides. The research on the effects of the environment on component cracking, was initiated in response to the determination that environmental effects were critical to several important cracking phenomena in LWR components. A major research program at Argonne National Laboratory (ANL) was initiated in 1979 to address pipe–cracking problems in boiling water reactors (BWRs). Since that time, in response to needs for additional research to support the Office of Nuclear Reactor Regulation (NRR) in assessing developing cracking problems in aging reactors, the focus of the project has shifted to address other problems in environmental cracking of LWR components. In recent years this activity has been supplemented by NRC participation in the Cooperative Irradiation Assisted Stress Corrosion Cracking Research (CIR) Program, a proprietary activity in which groups in several countries contribute money that is used to support research on irradiation–assisted stress corrosion cracking (IASCC) problems of common interest.

This project consists of several tasks with differing objectives, so the objectives are best described on a task–by–task basis:

Task 1: Environmental Effects on Fatigue Crack Initiation.

The objective of this task is to provide information on such topics as fatigue crack initiation in stainless steel (SS), and the synergistic effects of surface finish or loading sequence and environment on fatigue life. A comprehensive evaluation of SS fatigue test specimens will be performed to explain why environmental effects are more pronounced in low–dissolved oxygen (DO) than high–DO water. The contractor will review and evaluate issues related to environmental effects on fatigue as required by the NRC, and participate in ASME Code committees to incorporate the effects of LWR environments in fatigue life analyses.

Task 2: Evaluation of the Causes and Mechanisms of IASCC in BWRs.

This task will evaluate the susceptibility of austenitic SSs and their welds to IASCC as a function of fluence level, water chemistry, material chemistry, welding process, and fabrication history. It will provide data and technical support required for determination of inspection intervals, to help NRC address various issues that arise in license renewal or other licensee submittals. Crack growth rate (CGR) tests and slow strain rate tests (SSRTs) will be conducted on high–fluence model SSs from Halden Phase–I irradiations (carried out under NRC FIN W6610) to investigate the effects of material chemistry and irradiation level on the susceptibility of SSs to IASCC. CGR tests will be conducted on submerged arc (SA) and shielded metal arc (SMA) welds of Types 304 and 304L SS irradiated to 1.2×10^{21} n cm^{-2} in the Halden reactor to establish the effects of fluence level, material chemistry, and welding process on IASCC. Also, SSRTs and CGR tests will be carried out on grain boundary optimized (GBO) model SS alloys to study the effect of grain boundary geometry on IASCC and investigate the prospect of using GBO as a mitigative measure. Models and codes developed under CIR and from industry sources will be benchmarked and used in conjunction with this work.

Industry developed crack growth models will be analyzed and assessed. Also, the effectiveness of mitigative water chemistry measures, e.g., hydrogen water chemistry or noble metal additions, will be assessed. Much of this assessment will depend on data provided by industry, data available in the literature, and data developed as part of this task. However, for CGR models for irradiated materials, it is anticipated that relatively few data will be available because of the expense and difficulty of testing. Additional testing on nonirradiated materials will be performed to provide "limiting cases" against which the models can be tested. These tests will seek to determine the effects of Cr level in the steel and cold work on CGRs in austenitic SSs in LWR environments. This will be accomplished by procuring material and fabricating and testing compact–tension (CT) specimens from model SS alloys with lower Cr content and cold–worked (CW) Types 304L and 304 SS.

Task 3: Evaluation of Causes and Mechanisms of IASCC of Austenitic SS in PWRs.

The task will evaluate (a) the effects of very high fluence on CGRs, (b) neutron irradiation embrittlement, e.g., loss of fracture toughness, and (c) void swelling behavior in austenitic SSs. Tests will be conducted on material procured from the EBR–II reactor hexagonal fuel channels or irradiated in the BOR–60 reactor in Russia.

Task 4: Cracking of Nickel Alloys and Weldments.

The objective of this task is to provide the NRC with technical data on the implications of cracks in Ni–alloy components and weldments for residual life, inspection, and repair. Many reactor vessel internal components and their attachment welds, vessel penetrations, and piping butt welds are made of alloys such as Alloy 600, Alloy X750, and Alloy 182, which are susceptible to intergranular stress corrosion cracking (IGSCC). The causes and mechanisms of this cracking and the implications of microstructure, microchemistry, and surface finish for component life are also not well understood, and thus lead to greater uncertainty in licensee submissions that address issues such as damage accumulation and inspection intervals. The NRC research program will address these issues and provide data required to support staff assessment of industry CGR models, and potential crack detection and mitigation measures.

Task 5: Investigation of Other Modes of Degradation in High–Fluence Materials in PWR Environments.

Research at Saclay, France, has shown that gas generation in high fluence materials can produce unexpected changes in material behavior. Because studies on materials at high fluences and at temperatures of interest to LWRs are relatively limited, it is possible that additional degradation phenomena beyond those studied in detail in the other tasks could occur. The work in this task would seek to study, in cooperation with staff at Saclay and others in the CIR, the potential for other degradation phenomena.

2 Environmental Effects on Fatigue Crack Initiation in Carbon and Low–Alloy Steels and Austenitic Stainless Steels (O. K. Chopra)

2.1 Introduction

Cyclic loadings on a structural component occur because of changes in mechanical and thermal loadings as the system goes from one load set (e.g., pressure, temperature, moment, and force loading) to another. For each load set, an individual fatigue usage factor is determined by the ratio of the number of cycles anticipated during the lifetime of the component to the allowable cycles. Figures I–9.1 through I–9.6 of Appendix I to Section III of the ASME Boiler and Pressure Vessel Code specify fatigue design curves that define the allowable number of cycles as a function of applied stress amplitude. The cumulative usage factor (CUF) is the sum of the individual usage factors, and the ASME Code Section III requires that the CUF at each location must not exceed 1.

The ASME Code fatigue design curves, given in Appendix I of Section III, are based on strain–controlled tests of small polished specimens at room temperature in air. The design curves have been developed from the best–fit curves to the experimental fatigue–strain–vs.–life (ε–N) data that are expressed in terms of the Langer equation[1] of the form

$$\varepsilon_a = A1\ (N)^{-n1} + A2, \tag{1}$$

where ε_a is the applied strain amplitude, N is the fatigue life, and A1, A2, and n1 are coefficients of the model. Equation 1 may be written in terms of stress amplitude S_a instead of ε_a. The stress amplitude is the product of ε_a and elastic modulus E, i.e., $S_a = E\ \varepsilon_a$. The Code fatigue design curves are obtained from the best–fit curves of the experimental data by first adjusting for the effects of mean stress on fatigue life and then reducing the fatigue life at each point on the adjusted curve by a factor of 2 on strain (or stress) or 20 on cycles, whichever is more conservative.

As described in the Section III criteria document,[2] the factors of 2 and 20 were intended to account for data scatter (including material variability) and differences in surface condition and size between the test specimens and actual components. The factors are not safety margins but rather adjustment factors that should be applied to the small–specimen data to obtain reasonable estimates of the lives of actual reactor components. Although the Section III criteria document[2] states that these factors were intended to cover such effects as environment, Cooper,[3] in his comments regarding the initial scope and intent of the Section III fatigue design procedures, states that the term "atmosphere" was intended to reflect the effects of an industrial atmosphere in comparison with an air–conditioned laboratory. Subsection NB–3121 of Section III of the Code explicitly notes that the data used to develop the fatigue design curves did not include tests in the presence of corrosive environments that might accelerate fatigue failure. Article B–2131 in Appendix B to Section III states that the owner's design specifications should provide information about any reduction to fatigue design curves that is necessitated by environmental conditions.

Existing fatigue ε–N data illustrate potentially significant effects of LWR coolant environments on the fatigue resistance of carbon and low–alloy steels,[4–17] as well as austenitic stainless steels (SSs).[16–28] Under certain environmental and loading conditions, fatigue lives of carbon and low–alloy steels can be a factor of 70 lower in the coolant environment than in air.[5,14] Therefore, the margins in the ASME Code may be less conservative than originally intended.

Two approaches have been proposed for incorporating the environmental effects into ASME Section III fatigue evaluations for primary pressure boundary components in operating nuclear power plants: (a) develop new fatigue design curves for LWR applications, or (b) use an environmental correction factor to account for the effects of the coolant environment. In the first approach, environmentally adjusted fatigue design curves are developed from fits to the experimental data in LWR environments following the same procedures used to develop the current fatigue design curves of the ASME Code.[14,17,26] The second approach, proposed by Higuchi and Iida,[5] considers the effects of reactor coolant environments on fatigue life in terms of an environmental correction factor F_{en}, which is the ratio of fatigue life in air at room temperature to that in water under reactor operating conditions. To incorporate environmental effects into fatigue evaluations, the fatigue usage factor for a specific load set, based on the current Code design curves, is multiplied by the environmental correction factor.[11,14,17,26]

This report presents a critical review of the ASME Code fatigue design margins and an assessment of the conservatism in the current choice of design margins. The existing fatigue ε–N data for carbon and low–alloy steels and wrought and cast austenitic SSs have been evaluated to define the effects of key material, loading, and environmental parameters on the fatigue lives of these steels. Statistical models are presented for estimating their fatigue life as a function of material, loading, and environmental parameters. Both approaches for incorporating the effects of LWR environments into ASME Section III fatigue evaluations are described**.**

2.2 Experimental

Fatigue tests have been conducted to establish the effects of surface finish on the fatigue life of austenitic SSs and carbon and low–alloy steels in LWR environments. Tests were conducted on Types 304 and 316NG SS, A106–Gr B carbon steel, and A533–Gr B low–alloy steel; the chemical composition and heat treatments of the steels are given in Table 1.

Table 1. Chemical composition (wt.%) of austenitic and ferritic steels for fatigue tests

Material	Source	C	P	S	Si	Cr	Ni	Mn	Mo
Carbon Steel									
A106–Gr B[a]	ANL	0.290	0.013	0.015	0.25	0.19	0.09	0.88	0.05
	Supplier	0.290	0.016	0.015	0.24	–	–	0.93	–
Low–Alloy Steel									
A533–Gr B[b]	ANL	0.220	0.010	0.012	0.19	0.18	0.51	1.30	0.48
	Supplier	0.200	0.014	0.016	0.17	0.19	0.50	1.28	0.47
Austenitic Stainless Steel									
Type 304[c]	Supplier	0.060	0.019	0.007	0.48	18.99	8.00	1.54	0.44
Type 316NG[d]	Supplier	0.015	0.020	0.010	0.42	16.42	10.95	1.63	2.14

[a] 508–mm O.D. schedule 140 pipe fabricated by Cameron Iron Works, Heat J–7201. Actual heat treatment not known.
[b] 162–mm thick hot–pressed plate from Midland reactor lower head. Austenitized at 871–899°C for 5.5 h and brine quenched; then tempered at 649–663°C for 5.5 h and brine quenched. The plate was machined to a final thickness of 127 mm. The inside surface was inlaid with 4.8–mm weld cladding and stress relieved at 607°C for 23.8 h.
[c] 76 x 25 mm bar stock, Heat 30956. Solution annealed at 1050°C for 0.5 h.
[d] 25–mm–thick plate, Heat P91576. Solution annealed at 1050°C for 0.5 h.

Smooth cylindrical specimens, with 9.5–mm diameter and 19–mm gauge length, were used for the fatigue tests. The gauge section of the specimens was oriented along the axial directions of the carbon steel pipe and along the rolling direction for the bar and plates. The gauge length of all specimens was given a 1–μm surface finish in the axial direction to prevent circumferential scratches that might act as sites for crack initiation. For the roughness study, some specimens were intentionally roughened under controlled conditions, in a lathe, with 50–grit sandpaper to produce circumferential scratches. The average surface roughness (R_a) was 1.2 μm, and the root–mean–square (RMS) value of surface roughness (R_q) was 1.6 μm (61.5 micro–inch).

Tests in water were conducted in a 12–mL autoclave equipped with a recirculating water system. All tests were conducted at 288°C, with fully reversed axial loading and a triangular or sawtooth waveform. A detailed description of the test facility and test procedures has been presented earlier.[26,29]

2.3 Fatigue ε–N Data in LWR Environments

The existing fatigue ε–N data developed at various establishments and research laboratories worldwide have been compiled and categorized according to different test conditions. The fatigue data were obtained on smooth specimens tested under a fully reversed loading condition, i.e., load ratio R = –1; tests on notched specimens or at values of R other than –1 were excluded. In nearly all tests, fatigue life is defined as the number of cycles, N_{25}, for tensile stress to drop 25% from its peak or steady–state value; in some tests, life is defined as the number of cycles for peak tensile stress to decrease by 1–5%. Also, for fatigue tests on tube specimens, life was represented by the number of cycles to develop a leak.

2.3.1 Carbon and Low–Alloy Steels

In air, the fatigue lives of carbon and low–alloy steels depend on steel type, temperature, orientation (rolling or transverse), and strain rate. The fatigue life of carbon steels is a factor of ≈1.5 lower than that of low–alloy steels. For both steels, life is decreased by a factor of ≈1.5 when temperature is increased from room temperature to 288°C. In the temperature range of dynamic strain aging (200–370°C), these steels show negative sensitivity to strain rate, i.e., cyclic stresses increase with decreasing strain rate. Cyclic–stress–vs.–strain curves for carbon and low–alloy steels at 288°C have been developed as a function of strain rate.[12–17] The effect of strain rate on fatigue life is not clear. For some heats, life may be unaffected or decrease, but may increase for other heats. The ASME mean curve for low–alloy steels is in good agreement with the experimental data. The corresponding curve for carbon steels is somewhat conservative, especially at strain amplitudes of <0.2%.

The fatigue lives of carbon and low–alloy steels are reduced in LWR environments. Although the microstructures and cyclic–hardening behavior of carbon steels and low–alloy steels differ significantly, the effects of the environment on the fatigue life of these steels are very similar. The magnitude of the reduction depends on temperature, strain rate, DO level in water, and S content of the steel. The decrease is significant only when four conditions are satisfied simultaneously, viz., when the strain amplitude, temperature, and DO in water are above certain threshold values, and the strain rate is below a threshold value. For both steels, only a moderate decrease in life (by a factor of <2) is observed when any one of the threshold conditions is not satisfied. The S content in the steel is also important; its effect on life appears to depend on the DO level in water. The threshold values and the effects of the critical parameters on fatigue life are summarized below.

Strain: The results indicate that environmental effects on fatigue life are significant primarily during the tensile–loading cycle. A minimum total applied strain is required above which environmental effects on life are significant.[13–17] Even within a given loading cycle, environmental effects are significant at strain levels greater than this threshold value. Limited data suggest that the threshold value is ≈20% higher than the fatigue limit for the steel. Also, hold periods during peak tensile or compressive strain have no effect on the fatigue life of the steels.[14]

Strain Rate: When all other threshold conditions are satisfied, fatigue life decreases logarithmically with decreasing strain rate below 1%/s.[5,7,9] The effect of strain rate saturates at ≈0.001%/s.[12–17] When any one of the threshold conditions is not satisfied, e.g., DO <0.04 ppm or temperature <150°C, the

effects of strain rate are consistent with those observed in air. As a result, heats sensitive to strain rate in air show a decrease in life in water, although the decreases are smaller than those observed when the threshold conditions are met.

Temperature: Experimental data indicate a threshold temperature of 150°C, below which environmental effects on life either do not occur or are insignificant. When other threshold conditions are satisfied, fatigue life decreases linearly with temperature above 150°C and up to 320°C.[5,7,9] For service histories involving variable loading conditions, service temperature may be represented by the average of the minimum temperature or 150°C, whichever is higher, and the maximum temperature.[8]

Dissolved Oxygen in Water: When the other threshold conditions are satisfied, fatigue life decreases logarithmically with DO above 0.04 ppm; the effect saturates at ≈0.5 ppm DO.[7,9] Only a moderate decrease in life, i.e., a factor of <2, is observed at DO levels below 0.04 ppm.

Water Conductivity: The fatigue life of low–alloy steels decreases when the conductivity is increased.[30–32] The fatigue life of WB36 steel at 177°C in water with ≈8 ppm DO decreased by a factor of ≈6 when the conductivity of water was increased from 0.06 to 0.5 μS/cm.[31] A similar behavior has also been observed in studies on initiation of short cracks.[32]

Sulfur Content of Steel: The effect of S content on fatigue life appears to depend on the DO content of the water. When the threshold conditions are satisfied, the fatigue life decreases with increasing S content for DO levels ≤1.0 ppm. Limited data suggest that environmental effects on life saturate at an S content of ≈0.015 wt.%.[14] For DO levels >1.0 ppm, fatigue life seems to be relatively insensitive to S content in the range of 0.002–0.015 wt.%.[11]

Flow Rate: Recent data indicate that, under the environmental conditions typical of operating boiling water reactors (BWRs), environmental effects on the fatigue life of carbon steels are a factor of at least 2 lower at high flow rates (7 m/s) than at 0.3 m/s or lower.[33–35] The beneficial effects of increased flow rate are greater for high–S steels and at low strain rates.[33,34] A factor of 2 increase in fatigue life at 240°C has also been observed in component tests at KWU (Kraftwerk Union) laboratories using 180° bends of carbon steel tubing (0.025 wt.% S) where internal flow rates of up to 0.6 m/s were established.[35]

2.3.2 Austenitic Stainless Steels

In air environment, the fatigue lives of Types 304 and 316 SS are comparable; those of Type 316NG are slightly higher than Types 304 and 316 SS at high strain amplitudes. The results also indicate that the fatigue life of austenitic SSs in air is independent of temperature from room temperature to 427°C. Although the effect of strain rate on fatigue life seems to be significant at temperatures above 400°C, variations in strain rate in the range of 0.4–0.008%/s have no effect on the fatigue lives of SSs at temperatures up to 400°C.[36] The fatigue ε–N behavior of cast CF–8 and CF–8M SSs is similar to that of wrought austenitic SSs.[26] The ASME Code mean curve is not consistent with the existing fatigue ε–N data for austenitic SSs. At strain amplitudes <0.5%, the mean curve predicts significantly longer fatigue lives than those observed experimentally.[26,37]

The fatigue lives of austenitic SSs are also decreased in LWR environments. The magnitude of this reduction depends on strain amplitude, strain rate, temperature, DO level in the water, and possibly the composition and heat treatment of the steel.[16–28] The effects of LWR environments on fatigue lives of wrought materials are comparable for Types 304, 316, and 316NG SSs; effects on cast materials differ somewhat. As in the case of the carbon and low–alloy steels, fatigue life is reduced significantly only

when certain critical parameters meet certain threshold values. The critical parameters that influence fatigue life and the threshold values that are required for environmental effects to be significant are summarized below.

Strain Amplitude: As in the case of the carbon and low–alloy steels, environmental effects are significant primarily during the tensile–loading cycle. A minimum threshold strain is required for the environmentally induced decrease in fatigue lives of SS to occur. The threshold strain appears to be independent of material type (weld or base metal) and temperature in the range of 250–325°C, but it tends to decrease as the strain amplitude of the cycle is decreased.[23] The threshold strain appears to be related to the elastic strain range of the material.[23] Limited data indicate that hold periods during peak tensile or compressive strain have no effect on the fatigue life of austenitic SSs.[19,38]

Strain Rate: In low–DO PWR environments, fatigue life decreases logarithmically with decreasing strain rate below ≈0.4%/s; the effect of environment on fatigue life saturates at ≈0.0004%/s.[17–27] Only a moderate decrease in life is observed at strain rates >0.4%/s. In high–DO water, the effect of strain rate may be less pronounced than that in low–DO water. For cast SSs, the effect of strain rate on fatigue life is the same in low– and high–DO water and is comparable to that observed for the wrought SSs in low–DO water.[21,22]

Dissolved Oxygen in Water: In contrast to the behavior of carbon and low–alloy steels, the fatigue lives of nonsensitized wrought and cast austenitic SSs are decreased significantly even in low–DO (i.e., <0.01 ppm DO) water. The decrease in life is greater at low strain rates and high temperatures.[17–26] Environmental effects on the fatigue lives of these steels in high–DO water at temperatures above 150°C may be influenced by the composition and heat treatment of the steel. The fatigue lives of wrought SSs in high–DO water are either comparable to[21,22] or, in some cases, longer[26,27] than those in low–DO water.

In low–DO water, the fatigue lives of cast SSs are comparable to those for wrought austenitic SSs.[21–26] Limited data suggest that the fatigue lives of cast SSs in high–DO water are approximately the same as those in low–DO water.[26]

Water Conductivity: Limited data indicate that the fatigue life of SSs decreases when the conductivity is increased.[27] In high–DO water fatigue life decreases by a factor of ≈2 when the conductivity of water is increased from ≈0.07 to 0.4 μS/cm.

Temperature: The data suggest a lower threshold temperature of 150°C. Above this temperature the environment decreases life in low–DO water if the strain rate is below the threshold of 0.4%/s.[11,19] In the range of 150–325°C, the logarithm of fatigue life decreases linearly with temperature. Only a moderate decrease in life is observed in water at temperatures below the threshold value of 150°C. For variable–loading conditions, temperature may be represented by the average of the maximum temperature and the minimum temperature or 150°C, whichever is greater.[20]

Sensitization Anneal: In low–DO water, a sensitization anneal has no effect on the fatigue life of Types 304 and 316 SS, whereas, in high–DO water, environmental effects are enhanced in sensitized steels. For example, the fatigue life of sensitized steel is a factor of ≈2 lower than that of solution–annealed material in high–DO water.[21,22] Sensitization has little or no effect on the fatigue life of Type 316NG SS in low– and high–DO water.

Flow Rate: Limited data indicate that the water flow rate has no effect on the fatigue life of austenitic SSs in high–purity water at 289°C. The fatigue lives of Type 316NG at 0.6% strain amplitude

and 0.001%/s strain rate, in high–purity water with 0.2 or 0.05 ppm DO at 289°C, showed little or no change when the flow rate was increased from ≈10^{-5} to 10 m/s.[34] Because the mechanism of fatigue crack initiation in LWR environments appears to be different in SSs than in carbon steels, the effect of flow rate is also likely to be different.[27]

2.3.3 Effects of Surface Finish

Several fatigue tests have been conducted on rough specimens at 288°C in air and LWR environments. The results for A106–Gr B carbon steel and A533–Gr B low–alloy steel are shown in Figs. 1. The fatigue life of rough A106–Gr B specimens is a factor of 3 lower in air (triangles in Fig. 1a) compared with smooth specimens, and in high–DO water, it is the same. In low–DO water, the fatigue life of the roughened A106–Gr B specimen is slightly lower than that of smooth specimens. The effect of surface roughness on the fatigue life of A533–Gr B low–alloy steel is similar to that for A106–Gr B carbon steel; in high–DO water, the fatigue lives of both rough and smooth specimens are the same. The results for these steels are consistent with a mechanism of growth by a slip oxidation/dissolution process, which seems unlikely to be affected by surface finish. Because environmental effects are moderate in low–DO water, surface roughness would be expected to influence fatigue life.

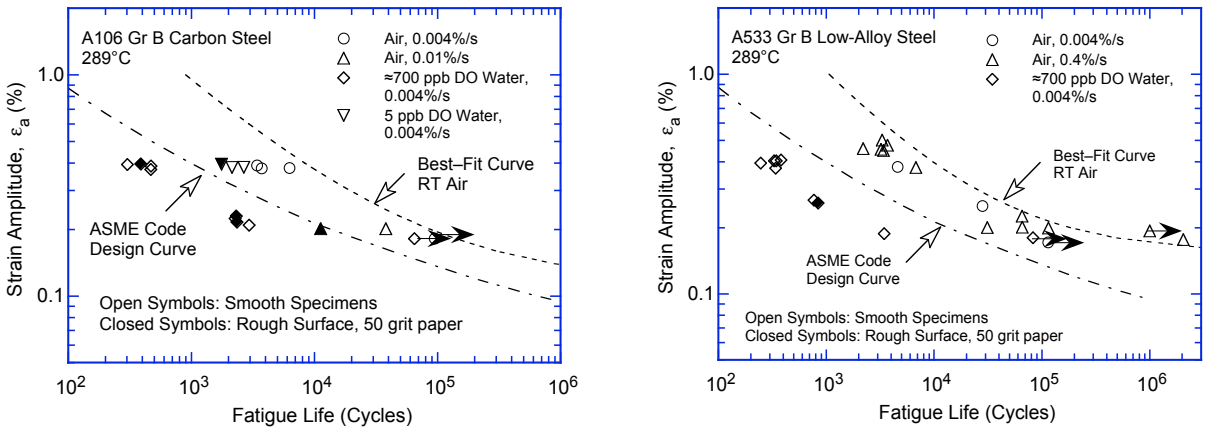

Figure 1. Effect of surface roughness on the fatigue life of (a) A106–Gr B carbon steel and (b) A533–Gr B low–alloy steel in air and high–purity water at 289°C.

The results for Types 316NG and 304 SS are shown in Figs. 2a and b, respectively. For both steels, the fatigue life of roughened specimens is lower than that of the smooth specimens in air and low–DO water environments. In high–DO water, the fatigue life is the same for rough and smooth specimens.

2.4 Statistical Model

Statistical models based on the existing fatigue ε–N data have been developed at ANL for estimating the fatigue lives of carbon and low–alloy steels and wrought and cast austenitic SSs in air and LWR environments.[14,17,26,28] In room–temperature air, the fatigue life N of carbon steels is represented by

$$\ln(N) = 6.564 - 1.975 \ln(\varepsilon_a - 0.113) \quad (2)$$

and that of low–alloy steels by

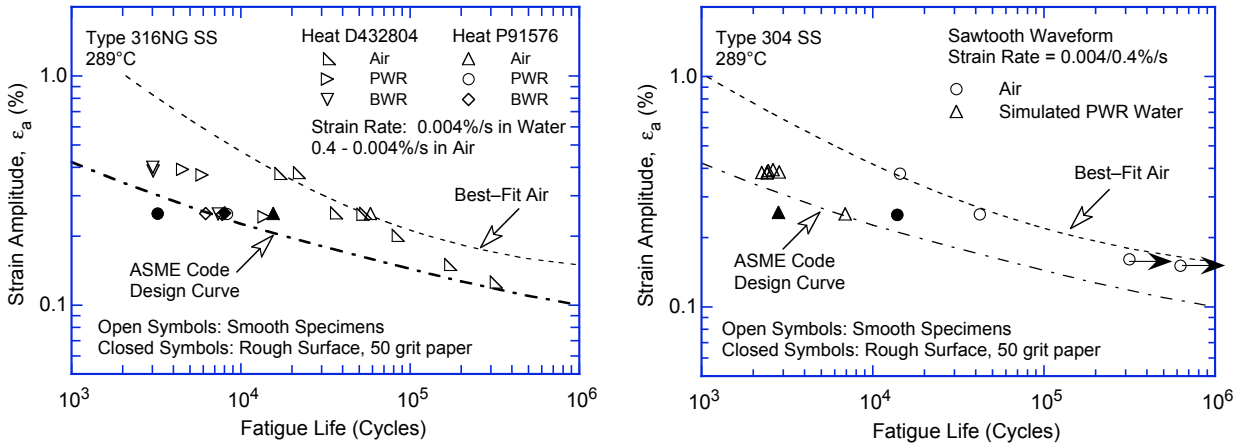

Figure 2. Effect of surface roughness on the fatigue life of (a) Type 316NG and (b) Type 304 SSs in air and high–purity water at 289°C.

$$\ln(N) = 6.627 - 1.808 \ln(\varepsilon_a - 0.151), \tag{3}$$

where ε_a is applied strain amplitude (%). In LWR environments, the fatigue life of carbon steels is represented by

$$\ln(N) = 6.010 - 1.975 \ln(\varepsilon_a - 0.113) + 0.101\, S^*\, T^*\, O^*\, \dot{\varepsilon}^* \tag{4}$$

and that of low–alloy steels, by

$$\ln(N) = 5.729 - 1.808 \ln(\varepsilon_a - 0.151) + 0.101\, S^*\, T^*\, O^*\, \dot{\varepsilon}^*, \tag{5}$$

where S^*, T^*, O^*, and $\dot{\varepsilon}^*$ are transformed S content, temperature, DO level, and strain rate, respectively, defined as:

$$\begin{aligned} S^* &= 0.015 && (DO > 1.0 \text{ ppm}) \\ S^* &= S && (DO \le 1.0 \text{ ppm and } S \le 0.015 \text{ wt.\%}) \\ S^* &= 0.015 && (DO \le 1.0 \text{ ppm and } S > 0.015 \text{ wt.\%}) \end{aligned} \tag{6}$$

$$\begin{aligned} T^* &= 0 && (T < 150°C) \\ T^* &= T - 150 && (T = 150–350°C) \end{aligned} \tag{7}$$

$$\begin{aligned} O^* &= 0 && (DO \le 0.04 \text{ ppm}) \\ O^* &= \ln(DO/0.04) && (0.04 \text{ ppm} < DO \le 0.5 \text{ ppm}) \\ O^* &= \ln(12.5) && (DO > 0.5 \text{ ppm}) \end{aligned} \tag{8}$$

$$\begin{aligned} \dot{\varepsilon}^* &= 0 && (\dot{\varepsilon} > 1\%/s) \\ \dot{\varepsilon}^* &= \ln(\dot{\varepsilon}) && (0.001 \le \dot{\varepsilon} \le 1\%/s) \\ \dot{\varepsilon}^* &= \ln(0.001) && (\dot{\varepsilon} < 0.001\%/s). \end{aligned} \tag{9}$$

In air at temperatures up to 400°C, the fatigue data for Types 304 and 316 SS are best represented by

$$\ln(N) = 6.703 - 2.030 \ln(\varepsilon_a - 0.126) \tag{10}$$

and those for Type 316NG, by

$$\ln(N) = 7.433 - 1.782 \ln(\varepsilon_a - 0.126). \quad (11)$$

The results indicate that, in LWR environments, the fatigue data for Types 304 and 316 SS are best represented by

$$\ln(N) = 5.675 - 2.030 \ln(\varepsilon_a - 0.126) + T' \dot{\varepsilon}' O' \quad (12)$$

and those of Type 316NG, by

$$\ln(N) = 7.122 - 1.671 \ln(\varepsilon_a - 0.126) + T' \dot{\varepsilon}' O', \quad (13)$$

where T', $\dot{\varepsilon}'$, and O' are transformed temperature, strain rate, and DO level, respectively, defined as:

$$\begin{aligned} T' &= 0 && (T < 150°C) \\ T' &= (T - 150)/175 && (150 \le T < 325°C) \\ T' &= 1 && (T \ge 325°C) \end{aligned} \quad (14)$$

$$\begin{aligned} \dot{\varepsilon} &= 0 && (\dot{\varepsilon} > 0.4\%/s) \\ \dot{\varepsilon} &= \ln(\dot{\varepsilon}/0.4) && (0.0004 \le \dot{\varepsilon} \le 0.4\%/s) \\ \dot{\varepsilon} &= \ln(0.0004/0.4) && (\dot{\varepsilon} < 0.0004\%/s) \end{aligned} \quad (15)$$

$$O' = 0.281 \quad \text{(all DO levels).} \quad (16)$$

These models are recommended for predicted fatigue lives $\le 10^6$ cycles. Note that in the above equations the fatigue life N represents the number of cycles needed to form a ≈3–mm deep crack. Equations 12 and 14–16 should also be used for cast austenitic SSs such as CF-3, CF-8, and CF–8M. Although the statistical models do not include the effects of flow rate on the fatigue life, the limited data available on the effects of flow rate suggest that under the conditions typical of operating BWRs, environmental effects on the fatigue life of carbon and low–alloy steels are a factor of ≈2 lower at high flow rates (7 m/s) than very low flow rates (0.3 m/s or lower).[33–35] Flow rate appears to have little or no effect on the fatigue life of austenitic SSs.[34] Also, as noted earlier, because the influence of DO level on the fatigue life of austenitic SSs is not well understood, these models may be conservative for some SSs in high–DO water. Also, because the effect of S on the fatigue life of carbon and low–alloy steels appears to depend on the DO level in water, Eqs. 2–9 may yield conservative estimates of fatigue life for low–S (<0.007 wt.%) steels in high–temperature water with >1 ppm DO.

2.5 Incorporating Environmental Effects

Two methods have been proposed for incorporating the effects of LWR coolant environments into the ASME Section III fatigue evaluations. In one case, new environmentally adjusted fatigue design curves are developed;[14–17,26,28] in the other, fatigue life correction factors F_{en} are used to adjust the fatigue usage values for environmental effects.[11,28,39,40]

2.5.1 Fatigue Design Curves

Fatigue design curves have been obtained from the statistical models, represented by Eqs. 2–9 for carbon and low–alloy steels, and by Eqs. 10, 12, 14–16 for austenitic SSs. To be consistent with the current ASME Code philosophy, the best–fit curves were first adjusted for the effect of mean stress by

using the modified Goodman relationship. The adjusted curves were then decreased by a factor of 2 on stress and 20 on cycles to obtain design curves. Although the current Code fatigue design curve for austenitic SSs does not include a mean stress correction, the new design curve does. Studies by Wire et al.[41] indicate an apparent reduction of up to 26% in strain amplitude in the low– and intermediate–cycle regime (i.e., $<10^6$ cycles) for a mean stress of 138 MPa.

Examples of fatigue design curves for carbon steels, low–alloy steels, and austenitic SS in LWR environments are shown in Fig. 3. For the environmentally adjusted fatigue design curves a minimum threshold strain is defined, below which environmental effects are modest. Based on the experimental

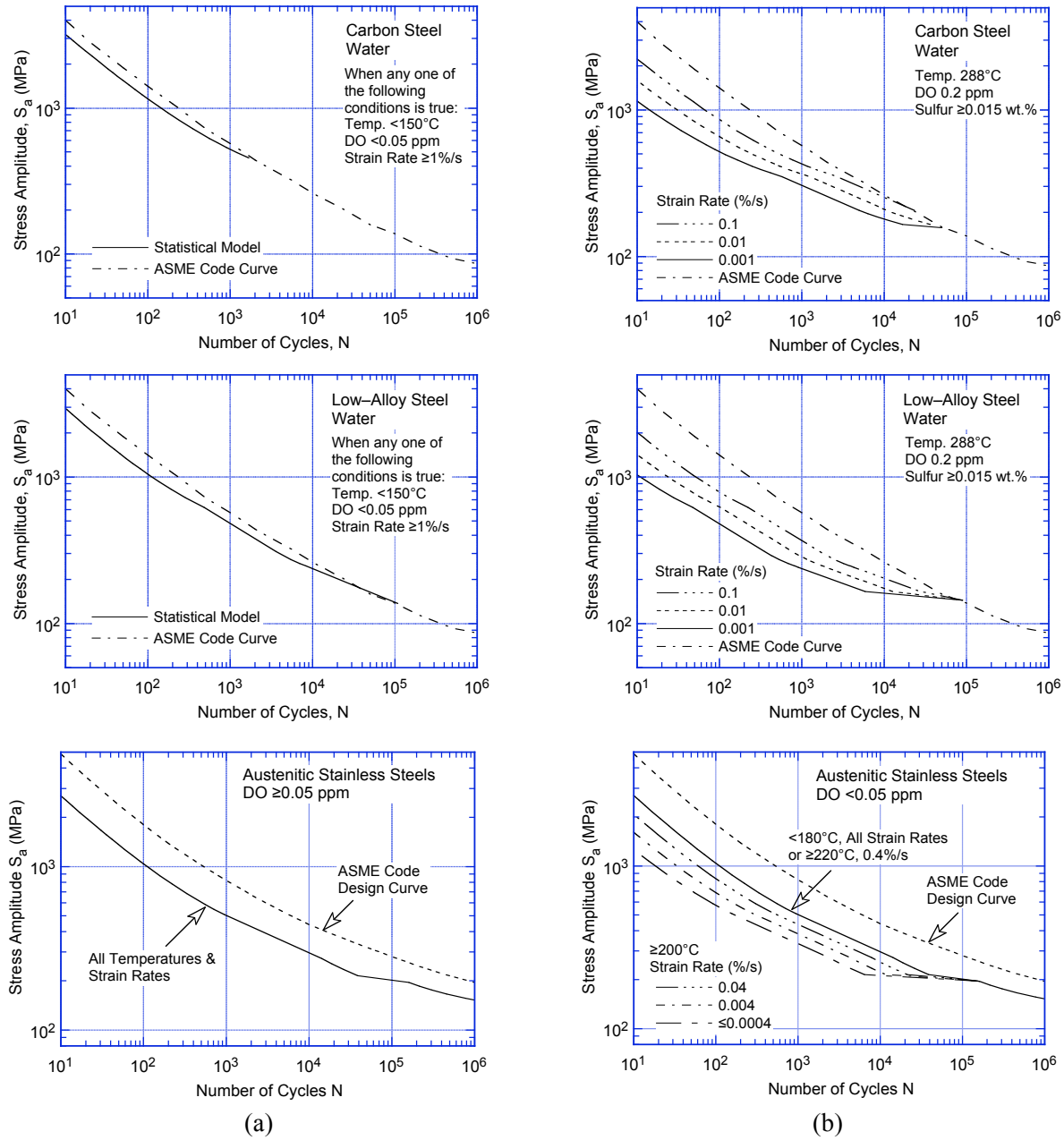

Figure 3. Fatigue design curves developed from the statistical model for carbon steels, low–alloy steels, and austenitic stainless steels in LWR environments under service conditions where (a) one or more critical threshold values are not satisfied, and (b) all threshold values are satisfied.

data, the pressure vessel research council (PVRC) steering committee for cyclic life environmental effects (CLEE)[40] has proposed a linear variation for the threshold strain; a lower strain amplitude below which environmental effects are insignificant, a slightly higher strain amplitude above which environmental effects decrease fatigue life, and a linear variation of environmental effects between the two values. The two strain amplitudes are 0.07 and 0.08% for carbon and low–alloy steels, and 0.10 and 0.11% for austenitic SSs (both wrought and cast SS). These threshold values were used to develop the curves in Fig. 3.

2.5.2 Fatigue Life Correction Factor

The effects of reactor coolant environments on fatigue life have also been expressed in terms of a fatigue life correction factor F_{en}, which is defined as the ratio of life in air at room temperature to that in water at the service temperature. Values of F_{en} can be obtained from the statistical model, where

$$\ln(F_{en}) = \ln(N_{RTair}) - \ln(N_{water}). \tag{17}$$

The fatigue life correction factor for carbon steels is given by

$$F_{en} = \exp(0.554 - 0.101\ S^*\ T^*\ O^*\ \dot{\varepsilon}^*), \tag{18}$$

for low–alloy steels, by

$$F_{en} = \exp(0.898 - 0.101\ S^*\ T^*\ O^*\ \dot{\varepsilon}^*), \tag{19}$$

and for austenitic SSs, by

$$F_{en} = \exp(1.028 - T'\ \dot{\varepsilon}'\ O'), \tag{20}$$

where the constants S^*, T^*, $\dot{\varepsilon}^*$, and O^* are defined in Eqs. 6–9, and T', $\dot{\varepsilon}'$, and O' are defined in Eqs. 14–16. A strain threshold is also defined, below which environmental effects are modest; the values are the same as those used in developing the fatigue design curves. To incorporate environmental effects into a Section III fatigue evaluation, the fatigue usage for a specific stress cycle based on the current Code fatigue design curve is multiplied by the correction factor.

2.6 Margins in ASME Code Fatigue Design Curves

Conservatism in the ASME Code fatigue evaluations may arise from (a) the fatigue evaluation procedures and/or (b) the fatigue design curves. The overall conservatism in ASME Code fatigue evaluations has been demonstrated in fatigue tests on components.[42,43] Mayfield et al.[42] have shown that, in air, the margins on the number of cycles to failure for elbows and tees were 40–310 and 104–510, respectively, for austenitic SS and 118–2500 and 123–1700, respectively, for carbon steel. The margins for girth butt welds were significantly lower at 6–77 for SS and 14–128 for carbon steel. Data obtained by Heald and Kiss[43] on 26 piping components at room temperature and 288°C showed that the design margin for cracking exceeds 20, and for most of the components it is greater than 100.

Deardorff and Smith[44] discussed the types and extent of conservatism present in the ASME Section III fatigue evaluation procedures and the effects of LWR environments on fatigue margins. The sources of conservatism in the procedures include the use of design transients that are significantly more severe than those experienced in service, conservative grouping of transients, and use of simplified

elastic–plastic analyses that result in higher stresses. The authors estimated that the ratio of the cumulative usage factors (CUFs) computed with the mean experimental curve in air and accurate values of the stress to the CUFs computed with the Code fatigue design curve were ≈60 and 90, respectively, for PWR and BWR nozzles. The reductions in these margins due to environmental effects were estimated to be factors of 5.2 and 4.6 for PWR and BWR nozzles, respectively. Thus, Deardorff and Smith[44] argue that, after accounting for environmental effects, factors of 12 and 20 on life for PWR and BWR nozzles, respectively, account for uncertainties due to material variability, surface finish, size, mean stress, and loading sequence.

However, other studies on piping and components indicate that the Code fatigue design procedures do not always ensure large margins of safety.[45,46] Southwest Research Institute performed fatigue tests in room–temperature water on carbon and low–alloy steels vessels with a 0.914–m diameter and 19–mm walls.[45] In the low–cycle regime, ≈5–mm–deep cracks were initiated slightly above (a factor of <2) the number of cycles predicted by the ASME Code design curve (Fig. 4a). Battelle–Columbus conducted tests on 203–mm or 914–mm carbon steel pipe welds at room temperature in an inert environment, and Oak Ridge National Laboratory (ORNL) performed four–point bend tests on 406–mm diameter Type 304 SS pipe removed from the C–reactor at the Savannah River site.[46] The results showed that the number of cycles to produce a leak was lower, and in some cases significantly lower, than that expected from the ASME Code fatigue design curves (Fig. 4a and b). Note that the Battelle and ORNL results represent a through–wall crack; the number of cycles to initiate a 3–mm crack may be a factor of 2 lower.

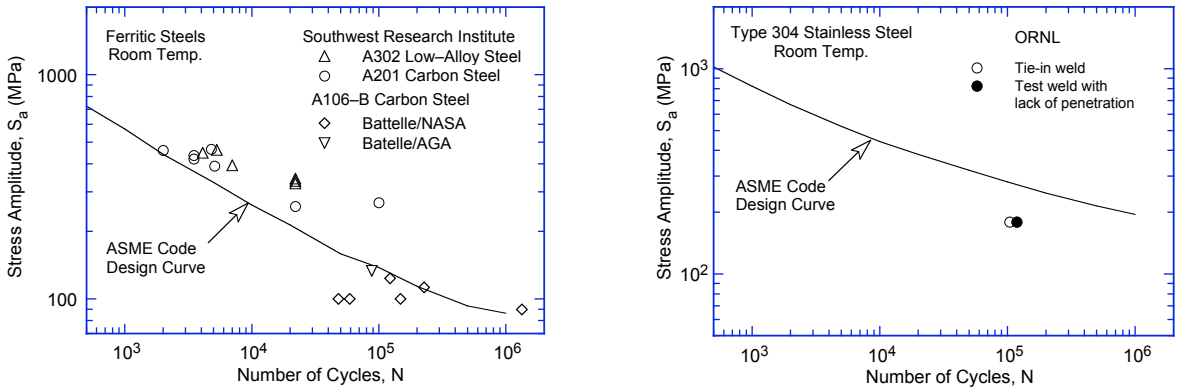

Figure 4. Fatigue data for (a) carbon and low–alloy steel and (b) Type 304 stainless steel components

Much of the margin in the current evaluations arises from design procedures (e.g., stress analysis rules and cycle counting) that, as discussed by Deardorff and Smith,[44] are quite conservative. However, the ASME Code permits new and improved approaches to fatigue evaluations (e.g., finite–element analyses, fatigue monitoring, and improved K_e factors) that can significantly decrease the conservatism in the current fatigue evaluation procedures.

The design margins of 2 and 20 on stress and cycles, respectively, were intended to cover the effects of variables that can influence fatigue life but were not investigated in the tests which provided the data for the curves. It is not clear whether the particular values of 2 and 20 that were chosen include possible conservatism. A study sponsored by the PVRC to assess the margins of 2 and 20 in fatigue design curves concluded that these margins could not be changed.[47]

The contributions of four groups of variables, namely, material variability and data scatter, size and geometry, surface finish, and loading sequence (Miner's rule), must be considered in developing the

fatigue design curves that are applicable to components. Data available in the literature have been reviewed in NUREG/CR–6717 to determine the effect of these variables on the fatigue life of components.[19]

2.6.1 Material Variability and Data Scatter

In developing fatigue design curves the effects of material variability and data scatter must be included to ensure that the curves not only describe the available test data well, but also adequately describe the fatigue lives of the much larger number of heats of material that are found in the field. The effects of material variability and data scatter are often evaluated by comparing the experimental data to a specific model for fatigue crack initiation, e.g., the best-fit to the data. The adequacy of the evaluation will then depend on the nature of the sample of data used in the analysis. For example, if most of the data are for a heat of material that has poor resistance to fatigue damage or obtained under loading conditions that show significant environmental effects, the results may be conservative for most of the materials or service conditions of interest. Conversely, if most data are for a heat of material with a high resistance to fatigue damage, the results could be nonconservative for many heats in service.

Another method to assess the effect of material variability and data scatter is by considering the best–fit curves determined from tests on individual heats of materials or loading conditions as samples of the much larger population of heats of materials and service conditions of interest. The fatigue behavior of each of the heats or loading conditions is characterized by the value of the constant term in the statistical models (e.g., Eq. 2), denoted as A. The values of A for the various data sets are ordered, and median ranks are used to estimate the cumulative distribution of A for the population.[48,49] The distributions were fit to lognormal curves. No rigorous statistical evaluation was performed, but the fits seem reasonable and describe the observed variability adequately. Results for carbon and low–alloy steels and austenitic SSs in air and water environments are shown in Fig. 5. Note that the mean values of A in Fig. 5 are slightly different from the values in Eqs. 2–5, 10, and 12, because they are based on a larger database. The statistical model expressions were obtained from Ref. 26 and have not been updated with the larger database. Such an update is planned after the final form of the model is established.

The values of A that describe the 5th percentile of these distributions give fatigue ε–N curves that are expected to bound the fatigue lives of 95% of the heats of the material. There are two sources of error in the distributions shown in Fig. 5. The mean and standard deviation of the population have to be estimated from the mean and standard deviation of the sample.[50] Confidence bounds can be obtained on the population mean and standard deviation in terms of the sample mean and standard deviation. Even this, however, does not fully address the uncertainty in the distribution, because of the large uncertainties in the sample values themselves, i.e., the "horizontal" uncertainty in the actual value of A for a heat of material as indicated by the error bars in Fig. 5.

A Monte Carlo analysis was used to address both sources of uncertainty. The results of the Monte Carlo analyses for the different steels are summarized in Tables 2–4 in terms of values for A that provide bounds for the portion of the population and the confidence that is desired in the estimates of the bounds. Note that with small sample sizes, demanding too high a confidence level can lead to very conservative estimates of the percentile values. Because the cumulative distributions in Fig. 5 do not properly account for all uncertainties, they should only be considered as a qualitative description of expected variation. Tables 2–4 should be used for quantitative estimates. For low–alloy steels, the 5th percentile value of parameter A at a 75% confidence level is 5.640 in air and 4.699 in LWR environments. From Fig. 5, the mean value of A for the sample is 6.366 and 5.824, respectively, in the two environments. Thus, for low–alloy steels, the 95/75 value of the margin to account for material variability and data scatter is 2.1 and 3.1

on life in air and water environments, respectively. The corresponding margins in air and water environments, respectively, are 2.3 and 2.9 for carbon steels, and 2.5 and 2.9 for SSs. Thus, average values of 2 and 3 on life in air and water environments, respectively, may be used to account for uncertainties due to material variability and data scatter. The estimated margins for these steels for different percentile and confidence levels may be determined from Tables 2–4 and the mean values of parameter A in Fig. 5. These margins are needed to provide reasonable confidence that the resulting life will be greater than that observed for 95% of the materials of interest.

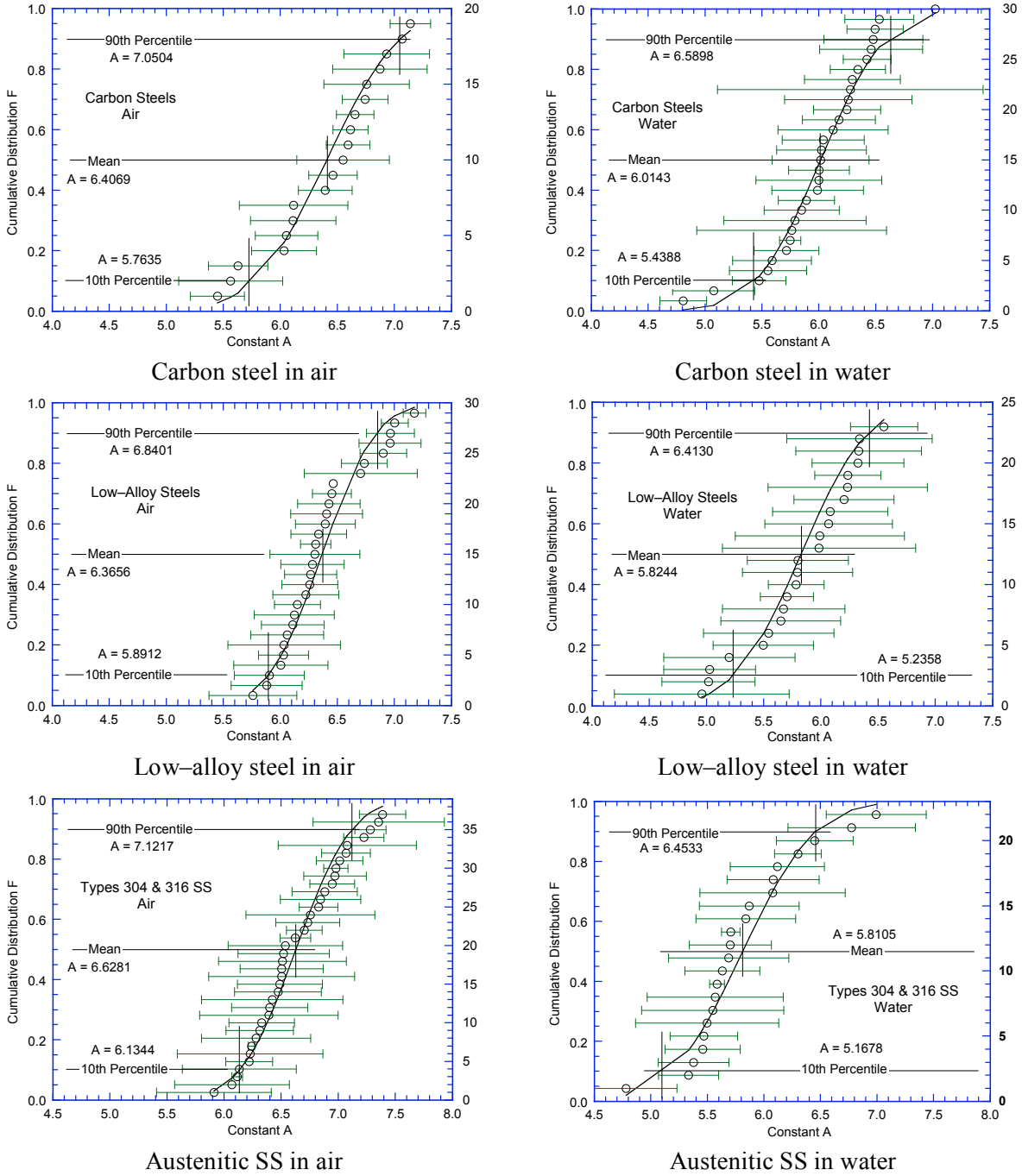

Figure 5. Estimated cumulative distribution of the parameter A in the statistical models for fatigue life for heats of carbon and low–alloy steels and austenitic SSs in air and water environments.

Table 2. Values of parameter A in the statistical model for carbon steels as a function of the percentage of the population bounded and the confidence level

Confidence Level	Percentage of Population Bounded (Percentile Distribution of A)				
	95 (5)	90 (10)	75 (25)	67 (33)	50 (50)
			Air Environment		
50	5.930	6.019	6.212	6.278	6.400
75	5.572	5.670	5.867	5.936	6.065
90	5.251	5.356	5.555	5.627	5.764
95	5.058	5.168	5.369	5.443	5.583
			LWR Environment		
50	5.300	5.444	5.675	5.767	5.948
75	4.959	5.119	5.370	5.466	5.652
90	4.652	4.836	5.095	5.195	5.386
95	4.468	4.651	4.931	5.033	5.227

Table 3. Values of parameter A in the statistical model for low–alloy steels as a function of the percentage of the population bounded and the confidence level

Confidence Level	Percentage of Population Bounded (Percentile Distribution of A)				
	95 (5)	90 (10)	75 (25)	67 (33)	50 (50)
			Air Environment		
50	5.912	6.000	6.180	6.242	6.370
75	5.640	5.738	5.927	5.992	6.119
90	5.395	5.503	5.700	5.768	5.893
95	5.249	5.362	5.563	5.633	5.758
			LWR Environment		
50	5.049	5.210	5.496	5.623	5.820
75	4.699	4.876	5.182	5.315	5.508
90	4.383	4.575	4.898	5.037	5.227
95	4.194	4.396	4.729	4.871	5.059

Table 4. Values of parameter A in the statistical model for austenitic stainless steels as a function of the percentage of the population bounded and the confidence level

Confidence Level	Percentage of Population Bounded (Percentile Distribution of A)				
	95 (5)	90 (10)	75 (25)	67 (33)	50 (50)
			Air Environment		
50	6.044	6.173	6.376	6.481	6.631
75	5.721	5.878	6.102	6.217	6.371
90	5.429	5.612	5.855	5.978	6.137
95	5.255	5.453	5.707	5.836	5.997
			LWR Environment		
50	5.135	5.288	5.538	5.636	5.805
75	4.755	4.928	5.193	5.297	5.468
90	4.412	4.604	4.882	4.992	5.164
95	4.208	4.410	4.696	4.809	4.983

2.6.2 Size and Geometry

The effect of specimen size on the fatigue life has been investigated for smooth specimens of various diameters in the range of 2–60 mm; the results have been summarized earlier.[17,27] The results indicate that the fatigue endurance limit decreases by ≈25% by increasing the specimen size from 2 to

16 mm but does not decrease further with larger sizes. A factor of ≈1.4 on cycles and a factor of ≈1.25 on strain can be used to account for size and geometry.

2.6.3 Surface Finish

Fatigue life is sensitive to surface finish; cracks can initiate at surface irregularities that are normal to the stress axis. The height, spacing, shape, and distribution of surface irregularities are important for crack initiation. Investigations of the effects of surface roughness on the low–cycle fatigue of Type 304 SS in air at 593°C indicate that fatigue life decreases as surface roughness increases.[51,52] The effect of roughness on crack initiation $N_i(R)$ is given by

$$N_i(R_q) = 1012\ R_q^{-0.21}, \tag{21}$$

where the RMS value of surface roughness (R_q) is in micrometers. An R_q of 4 μm represents the maximum surface roughness for drawing/extrusion, grinding, honing, and polishing processes and a mean value for the roughness range for milling or turning processes.[53] For SSs, an R_q of 4 μm in Eq. 21 (R_q of a smooth polished specimen is ≈0.0075 μm) would decrease fatigue life by a factor of 3.7.[51] A study of the effect of surface finish on fatigue life of carbon steel in room–temperature air showed a factor of 2 decrease in life when the average surface roughness R_a was increased from 0.3 to 5.3 μm.[54]

The results from the present study are consistent with Eq. 21. From Eq. 21, an R_q of 1.6 μm corresponds to a factor of 3.1 decrease in fatigue life for the roughened specimen. The results suggest that factors of ≈3 on cycles would account for effects of surface finish on the fatigue life of austenitic SSs in both air and water environments and for carbon and low–alloy steels in air. A factor of 3 decrease in life corresponds to a factor of ≈1.3 on strain.* For carbon and low–alloy steels, the effect of surface finish is lower in LWR environments.

The decrease in fatigue life of both carbon and low–alloy steels and austenitic SSs is caused primarily by the effect of the environment on the growth of microstructurally small cracks and, to a lesser extent, on the growth of mechanically small cracks.[55,56] The observed effects of surface finish on the fatigue life of SSs and carbon and low–alloy steels in LWR environments appear to be consistent with the hypothesis that the mechanisms of the growth of microstructurally small cracks are different in austenitic SSs and carbon or low–alloy steels, although other explanations are also possible. The fact that the fatigue life of carbon and low–alloy steels is unaffected by surface finish is consistent with the possibility of a mechanism like slip/dissolution which is less dependent on the stress level. The reduction in life of SSs is consistent with a mechanism that is enhanced by higher stresses, e.g., hydrogen–enhanced crack growth mechanism.

2.6.4 Loading Sequence

Fatigue life has conventionally been divided into two stages: initiation, expressed as the cycles required to form microcracks on the surface; and propagation, expressed as cycles required to propagate the surface cracks to engineering size. During cyclic loading of smooth test specimens, surface cracks 10 μm or longer form quite early in life (i.e., <10% of life) at surface irregularities or discontinuities either already in existence or produced by slip bands, grain boundaries, second–phase particles, etc.[14,55]

---

* Considering the factor of 20 on cycles to be equivalent to the factor of 2 on strain, the factor applied on strain (K_S) is obtained from the factor applied on cycles (K_N) by using the relationship $K_S = (K_N)^{0.2326}$.

Consequently, fatigue life may be considered to be composed entirely of propagation of cracks from 10 to 3000 μm long.

A schematic illustration of the two stages, i.e., initiation and propagation, of fatigue life is shown in Fig. 6. The initiation stage involves growth of microstructurally small cracks (MSCs), characterized by decelerating crack growth (Region AB in Fig. 6a). The propagation stage involves growth of mechanically small cracks, characterized by accelerating crack growth (Region BC in Fig. 6a). The growth of MSCs is very sensitive to microstructure.[55] Fatigue cracks greater than the critical length of MSCs show little or no influence of microstructure, and are termed mechanically small cracks. Mechanically small cracks correspond to Stage II (tensile) cracks, which are characterized by striated crack growth, with a fracture surface normal to the maximum principal stress. Various criteria, summarized in Ref. 17, have been used to define the crack length for transition from microstructurally to mechanically small crack; the transition crack length is a function of applied stress (σ) and microstructure of the material; actual values may range from 150 to 250 μm.

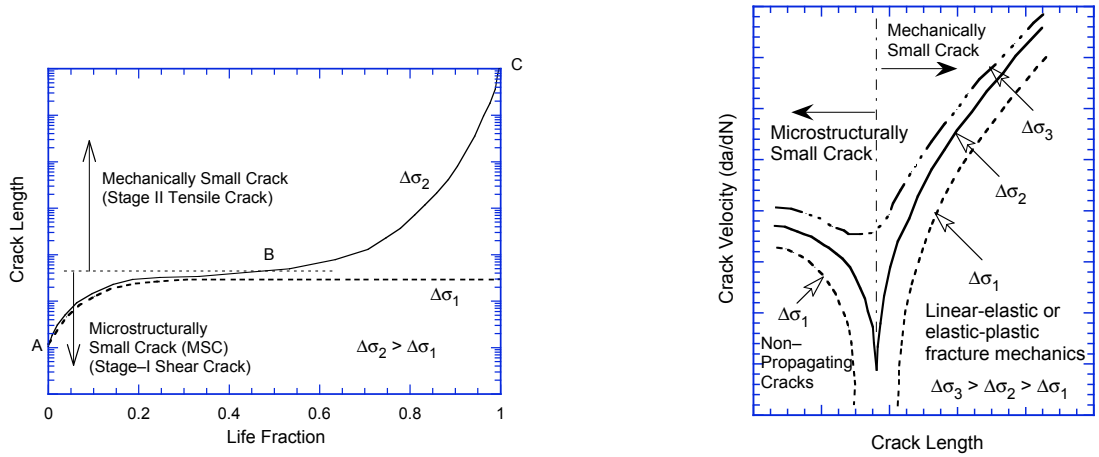

Figure 6. Schematic illustration of (a) growth of short cracks in smooth specimens as a function of fatigue life fraction and (b) crack velocity as a function of crack length. LEFM = linear elastic fracture mechanics.

At low stress levels ($\Delta\sigma_1$), the transition from MSC growth to accelerating crack growth does not occur. This circumstance represents the fatigue limit for the smooth specimen. Although cracks can form below the fatigue limit, they can grow to engineering size only at stresses greater than the fatigue limit. Note that the fatigue limit for a material is applicable only for constant loading conditions. Under variable loading conditions encountered during service of power plants, cracks created by growth of MSCs at high stresses ($\Delta\sigma_3$) to lengths larger than the transition crack length can increase at stresses below the fatigue limit ($\Delta\sigma_1$).

The effects of variable amplitude loading of smooth specimens are well known.[57–61] The presence of a few cycles at high strain amplitude in a loading sequence causes the fatigue life at smaller strain amplitude to be significantly lower than that at constant amplitude loading. Studies on fatigue damage in Type 304 SS under complex loading histories[61] indicate that the loading sequence of decreasing strain levels (i.e., high strain level followed by low strain level) is more damaging than that of increasing strain levels. The fatigue life of the steel decreased by a factor of 2–4 under a decreasing–strain sequence. In another study, the fatigue limit of medium carbon steels was lowered even after low–stress high–cycle fatigue; the higher the stress, the greater the decrease in fatigue threshold.[62] In general, the mean fatigue

ε–N curves are lowered to account for damaging cycles that occur below the constant–amplitude fatigue limit of the material. A factor of 1.5–2.5 on cycles and 1.3–1.6 on strain may be used to incorporate the effects of load histories on fatigue life.

2.6.5 Fatigue Design Curve Margins Summarized

The subfactors that are needed to account for the effects of various material, loading, and environmental variables on fatigue life are summarized in Table 5. As shown by "total adjustment," a factor of at least 12.5 on cycles with respect to the mean ε–N curve for laboratory test specimens in air is needed to account for the effects of data scatter, material variability, component size, surface finish, and loading history. In LWR environments, a factor of at least 19 on cycles with respect to the mean ε–N curve for laboratory test specimens is needed for austenitic SSs and at least 10 on cycles for carbon and low–alloy steels.

The factors on strain are needed primarily to account for the variation in the fatigue limit of the material caused by material variability, component size and surface finish, and load history. Because these variables affect life through their influence on the growth of short cracks (<100 μm), the adjustment on strain to account for such variations is typically not cumulative, i.e., the portion of the life can only be reduced by a finite amount. Thus, it is controlled by the variable that has the largest effect on life. In relating the fatigue lives of laboratory test specimens to those of actual reactor components, a factor of ≈1.7 on strain with respect to the mean ε–N curve for laboratory test specimens is needed to account for the uncertainties associated with material variability, component size, surface finish, and load history.

These results suggest that the current ASME Code requirements of a factor of 2 on stress and 20 on cycle to account for differences and uncertainties in fatigue life that are associated with material and loading conditions are quite reasonable, and do not contain excess conservatism that can be assumed to account for the effects of LWR environments. They thus provide appropriate margins for the development of design curves from mean data curves for small specimens in LWR environments.

Table 5. Factors to be applied to mean ε–N curve

Parameter	Factor on Life (Air)	Factor on Life (Water)		Factor on Strain or Stress
		Stainless Steels	Carbon/Low-Alloy Steels	
Material variability & experimental scatter	2.0	3.0	3.0	1.2–1.7
Size effect	1.4	1.4	1.4	1.25
Surface finish	3.0	3.0	1.6	1.6
Loading history	1.5–2.5	1.5–2.5	1.5–2.5	1.3–1.6
Total adjustment	12.5–21.0	19.0–31.0	10.0–17.0	1.6–1.7

3 Irradiation–Assisted Stress Corrosion Cracking of Austenitic Stainless Steel in BWRS

The susceptibility of austenitic SSs and their welds to IASCC as a function of the fluence level, water chemistry, material chemistry, welding process, and fabrication history is being evaluated. Crack growth rate (CGR) tests and slow strain rate tests (SSRTs) are being conducted on model SSs, irradiated at ≈288°C in a helium environment in the Halden boiling heavy water reactor, to investigate the effects of material chemistry and irradiation level on the susceptibility of SSs to IASCC. Crack growth tests will be conducted on irradiated specimens of submerged arc (SA) and shielded metal arc (SMA) welds of Types 304 and 304L SS to establish the effects of fluence level, material chemistry, and welding process on IASCC. Models and codes developed under CIR and from industry sources will be benchmarked and used in conjunction with this work. However, for crack–growth rate models for irradiated materials it is anticipated that relatively few data will be available because of the expense and difficulty of testing. Additional testing on nonirradiated materials will be performed to provide "limiting cases" against which the models can be tested. These tests will seek to determine the effects of Cr level in the steel and cold work on CGRs in austenitic SSs in LWR environments.

During this reporting period SSRT tests were conducted on specimens irradiated to a "high-fluence" level of ≈2.0 x 10^{21} n cm^{-2} (E > 1 MeV) and CGR tests were conducted on Types 304 and 316 SS, irradiated up to 2.0 x 10^{21} n cm^{-2} (E > 1 MeV), in BWR environments at ≈289°C.

3.1 Slow-Strain-Rate-Tensile Test of Model Austenitic Stainless Steels Irradiated in the Halden Reactor (H. M. Chung, R. V. Strain, and R. W. Clark)

3.1.1 Introduction

Failures of some BWR and PWR core internal components have been observed after accumulation of fast neutron fluences higher than ≈0.5 x 10^{21} n cm^{-2} (E >1 MeV) (≈0.7 dpa) in BWRs and at fluences approximately an order of magnitude higher in PWRs. The general pattern of the observed failures indicates that as nuclear plants age and fluence increases, various nonsensitized austenitic stainless steels (SSs) become susceptible to intergranular (IG) failure. Failure of welded components (such as core shrouds fabricated from Type 304 or 304L SS) has also been observed in many BWRs, usually at fluence levels significantly lower than the threshold fluence for the solution-annealed base-metal components.

Although most failed components can be replaced, some safety–significant structural components (e.g., the BWR top guide, core shroud, and core plate) would be very difficult or costly to replace. Therefore, the structural integrity of these components has been a subject of concern, and extensive research has been conducted to provide an understanding of this type of degradation, which is commonly known as irradiation-assisted stress corrosion cracking (IASCC).[63–84]

Irradiation produces profound effects on local coolant water chemistry and component microstructure. Neutron irradiation causes alteration of microchemistry, microstructure, and mechanical properties of the core internal components, which are usually fabricated from ASTM Types 304, 304L, 316, or 348 SS. It produces defects, defect clusters, and defect-impurity complexes in grain matrices and alters the dislocation and dislocation loop structures, leading to radiation-induced hardening, and in many cases, flow localization via dislocation channeling. It also leads to changes in the stability of second–phase precipitates and the local alloy chemistry near grain boundaries, precipitates, and defect clusters. Grain–boundary microchemistry significantly different from bulk composition can be produced in

association with not only radiation–induced segregation, but also thermally driven equilibrium and nonequilibrium segregation of alloying and impurity elements.

Irradiation–induced grain–boundary depletion of Cr has been considered for many years to be the primary metallurgical process that leads IASCC in BWRs. One of the most important factors that seem to support the Cr–depletion mechanism is the observation that the dependence on water chemistry (i.e., oxidizing potential) of intergranular stress corrosion cracking (IGSCC) of nonirradiated thermally sensitized material and of IASCC of BWR–irradiated solution–annealed material is similar.[63–65] Many investigators have also suggested that radiation–induced segregation of ASTM–specified impurities such as Si and P and other minor impurities not specified in the ASTM specification[66–83] has a role in the IASCC process. However, the exact mechanism of IASCC still remains unknown.

In general, IASCC is characterized by strong heat-to-heat variation in susceptibility, even among materials of virtually identical chemical compositions. This suggests that the traditional interpretation based on the role of grain-boundary Cr depletion alone may not completely explain the IASCC mechanism. An irradiation test program is being conducted to investigate systematically the effects of alloying and impurity elements (Cr, Ni, Si, P, S, Mn, C, N, and O) on the susceptibility of austenitic stainless steels to IASCC at several fluence levels.

In previous studies, SSRT tests and fractographic analysis were conducted on model austenitic SS alloys irradiated at 289°C to a "low-fluence" level of ≈0.3 x 10^{21} n cm^{-2} (E > 1 MeV) (≈0.43 dpa), and a "medium-fluence" level of ≈0.9 x 10^{21} n cm^{-2} (E > 1 MeV) (≈1.3 dpa).[84,85] This report describes results of SSRT tests and post–test fractographic analysis performed on 11 SS heats irradiated to a "high-fluence" level of ≈2.0 x 10^{21} n cm^{-2} (E > 1 MeV) (≈2.9 dpa). Ten of the 11 heats were austenitic SS and one was austenitic-ferritic SS containing ≈3 vol.% ferrite of globular shape.

3.1.2 Experimental Procedure

To systematically investigate the effects of Cr, Ni, Si, P, S, Mn, C, N, and O, model austenitic SS alloys were obtained from commercial sources and through production of laboratory heats. Details of the test matrix and experimental procedures have been given in an earlier report.[23] The chemical compositions of the materials in the test matrix are given in Table 6. Sheet SSRT specimens (thickness of 0.76 mm) were machined from solution-annealed and water-quenched plates or thick large-diameter tubes. The machined and cleaned specimens were irradiated at 289°C in helium in the Halden Reactor to ≈2.0 x 10^{21} n cm^{-2} (E > 1 MeV). Fast neutron flux ranged from 1.8 x 10^{13} to 3.3 x 10^{13} n cm^{-2} s^{-1}.

Slow-strain-rate tensile tests were conducted at 289°C in high-purity deionized water that contained ≈8 ppm DO. Conductivity at 23°C and pH of the water were kept at ≈0.07–0.10 μS cm^{-1} and 6.3–6.8, respectively. Strain rate was held constant at 1.65 x 10^{-7} s^{-1}. During the tests the electrochemical potential (ECP) was measured on an electrode on the effluent side of the circulating water loop at a regular interval.

In parallel to the SSRT tests in 289°C water, the bend fracture of selected specimens was investigated. After completion of an SSRT test in 289°C water, a broken portion of the specimen was fractured in air at 23°C by bending as illustrated in Fig. 7. After fracture, fractographic analysis was performed in a shielded scanning electron microscope (SEM).

Table 6. Elemental composition of 27 commercial and laboratory-fabricated austenitic SSs irradiated in the Halden Reactor

ANL	Source	Composition (wt.%)										
ID[a]	Heat ID	Ni	Si	P	S	Mn	C	N	Cr	O	B	Mo or Nb
C1	DAN-70378	8.12	0.50	0.038	0.002	1.00	0.060	0.060	18.11	-	<0.001	-
L2	BPC-4-111	10.50	0.82	0.080	0.034	1.58	0.074	0.102	17.02	0.0065	<0.001	-
C3	PNL-C-1	8.91	0.46	0.019	0.004	1.81	0.016	0.083	18.55	-	<0.001	-
L4	BPC-4-88	10.20	0.94	0.031	0.010	1.75	0.110	0.002	15.80	-	<0.001	-
L5	BPC-4-104	9.66	0.90	0.113	0.028	0.47	0.006	0.033	21.00	-	<0.001	-
L6	BPC-4-127	10.00	1.90	0.020	0.005	1.13	0.096	0.087	17.10	0.0058	<0.001	-
L7	BPC-4-112	10.60	0.18	0.040	0.038	1.02	0.007	0.111	15.40	0.0274	<0.001	-
L8	BPC-4-91	10.20	0.15	0.093	0.010	1.85	0.041	0.001	18.30	-	<0.001	-
C9	PNL-C-6	8.75	0.39	0.013	0.013	1.72	0.062	0.065	18.48	-	<0.001	-
C10	DAN-23381	8.13	0.55	0.033	0.002	1.00	0.060	0.086	18.19	-	<0.001	-
L11	BPC-4-93	8.15	0.47	0.097	0.009	1.02	0.014	0.004	17.40	-	<0.001	-
C12	DAN-23805	8.23	0.47	0.018	0.002	1.00	0.060	0.070	18.43	-	<0.001	-
L13	BPC-4-96	8.18	1.18	0.027	0.022	0.36	0.026	0.001	17.40	-	<0.001	-
L14	BPC-4-129	7.93	1.49	0.080	0.002	1.76	0.107	0.028	15.00	0.0045	<0.001	-
L15	BPC-4-126	8.00	1.82	0.010	0.013	1.07	0.020	0.085	17.80	0.0110	<0.001	-
C16	PNL-SS-14	12.90	0.38	0.014	0.002	1.66	0.020	0.011	16.92	0.0157	<0.001	-
L17	BPC-4-128	8.00	0.66	0.090	0.009	0.48	0.061	0.078	15.30	0.0090	<0.001	-
L18	BPC-4-98	8.13	0.14	0.016	0.033	1.13	0.080	0.001	18.00	-	<0.001	-
C19	DAN-74827	8.08	0.45	0.031	0.003	0.99	0.060	0.070	18.21	0.0200	<0.001	-
L20	BPC-4-101	8.91	0.017	0.010	0.004	0.41	0.002	0.002	18.10	0.0940	<0.001	-
C21	DAN-12455	10.24	0.51	0.034	0.001	1.19	0.060	0.020	16.28	-	<0.001	Mo 2.08
L22	BPC-4-100	13.30	0.024	0.015	0.004	0.40	0.003	0.001	16.10	-	<0.001	Mo 2.04
L23	BPC-4-114	12.04	0.68	0.030	0.047	0.96	0.043	0.092	17.30	0.0093	<0.001	Nb 1.06
L24	BPC-4-105	12.30	0.03	0.007	0.005	0.48	0.031	0.002	16.90	0.0129	<0.001	Nb 1.72
L25C3	BPC-4-133	8.93	0.92	0.020	0.008	1.54	0.019	0.095	17.20	0.0085	0.010	-
L26C19	BPC-4-131	8.09	0.79	0.004	0.002	0.91	0.070	0.089	17.20	0.0080	<0.001	-
L27C21	BPC-4-132	10.30	0.96	0.040	0.002	0.97	0.057	0.019	15.30	0.0058	0.030	Mo 2.01

[a]The first letters "C" or "L" denotes, respectively, a commercial or laboratory heat.

In addition to the fracture testing, a few specimens sectioned from BWR neutron absorber tubes fabricated from two heats of 304 SS were analyzed by Auger electron spectroscopy (AES) to determine grain-boundary segregation of S and C. The AES analysis was performed in a JEOL JAMP-10 scanning AEM equipped with automated Ar sputtering and depth-profiling devices.

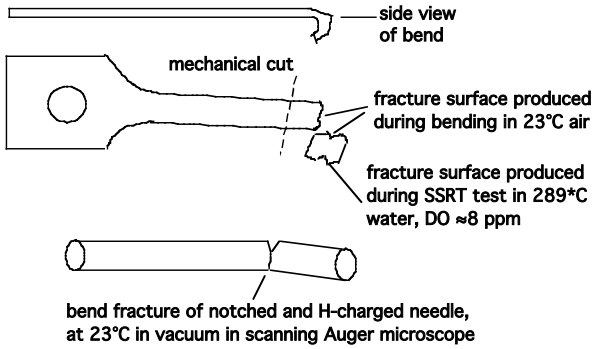

Figure 7.
Schematic illustration of bending fracture in air and in vacuum.

3.1.3 Results of SSRT Testing

Table 7 summarizes the results of the SSRT testing in 289°C water (DO ≈8 ppm) and the corresponding SEM fractography. Table 8 compares the SEM fractography of specimens fractured in SSRT tests in 289°C water with the fractography of specimens fractured by bending in 23°C air, with or

without previous exposure to the SSRT test in 289°C water. Chemical composition of the heats, measured before irradiation, is also given in the table.

Table 7. Results of slow-strain-rate tensile test[a] and fractographic analysis on austenitic stainless steels irradiated to ≈3 dpa in Halden Reactor at 289°C in helium.

			Feedwater Chemistry			SSRT Properties				Fracture Behavior		
Test Spec. ID	SSRT No.	DO Conc. (ppm)	Average ECP (mV SHE)	Cond. At 23°C (μS cm^{-1})	pH at 25°C	Yield Stress (MPa)	Max. Stress (MPa)	Uniform Elong. (%)	Total Elong. (%)	TGSCC (%)	IGSCC (%)	TG + IGSCC (%)
L4-03	HR-45	9.0	+198	0.09	6.5	876	1068	2.49	3.27	5	95	100
C12-03	HR-46	8.0	+208	0.09	6.5	922	996	1.28	2.73	8	2	10
C9-03	HR-47	8.0	+212	0.11	6.5	Early failure during test in water				6	94	100
L5-03	HR-48	8.0	+204	0.10	6.5	953	985	0.59	2.97	2	4	6
C19-03	HR-49	8.0	+171	0.11	6.5	787	801	0.89	3.32	2	62	64
C16-03	HR-50	7.9	+202	0.10	6.5	766	803	0.83	1.84	2	29	31
C10-03	HR-51	8.0	+167	0.11	6.5	1062	1065	3.15	4.51	3	0	3
L18-03	HR-52	8.0	+169	0.11	6.5	795	779	0.35	1.75	5	86	91
L13-03	HR-53	–	–	Brittle fracture during test preparation					–	–	–	–
C1-03	HR-54	7.8	+161	0.10	6.5	802	833	3.38	5.27	2	0	2
C3-03	HR-55	7.8	+160	0.10	6.5	796	826	5.05	7.31	0	26	26
C21-03	HR-56	7.6	+156	0.10	6.5	893	924	1.89	4.85	2	1	3
L8-03	HR-57	–	–	Failure during test preparation					–	–	–	–

[a]Test at 289°C at strain rate of 1.65 x 10^{-7} s^{-1} in BWR-like water; DO ≈ 8 ppm.

Table 8. Composition (in wt.%) of austenitic stainless steels irradiated at 289°C in helium to 3 dpa in the Halden Reactor, correlated with results of SEM fractography after SSRT test in 289°C water and bend test in 23°C air.

Test Speci. ID[a]	Ni	Si	P	S	Mn	C	N	Cr	O	% IGSCC SSRT in 289°C water	% IGC, bend in 23°C air after SSRT in 289°C water	% IGC, bend in 23°C air without exposure to water
L4-03	10.20	0.94	0.031	0.010	1.75	0.110	0.002	15.80	0.0037	95	–	–
C12-03	8.23	0.47	0.018	0.002	1.00	0.060	0.070	18.43	0.0102	2	92	–
C9-03	8.75	0.39	0.013	0.013	1.72	0.062	0.065	18.48	0.0102	94	0	–
L5-03	9.66	0.90	0.113	0.028	0.47	0.006	0.033	21.00	0.0068	4	–	–
C19-03	8.08	0.45	0.031	0.003	0.99	0.060	0.070	18.21	0.0200	62	28	–
C16-03	12.90	0.38	0.014	0.002	1.66	0.020	0.011	16.92	0.0150	29	0	–
C10-03	8.13	0.55	0.033	0.002	1.00	0.060	0.086	18.19	0.0074	0	87	–
L18-03	8.13	0.14	0.016	0.033	1.13	0.080	0.001	18.00	0.0055	86	0	–
L13-03	8.18	1.18	0.027	0.022	0.36	0.026	0.001	17.40	0.0042	–	–	95
C1-03	8.12	0.50	0.038	0.002	1.00	0.060	0.060	18.11	0.0102	0	53	–
C3-03	8.91	0.46	0.019	0.004	1.81	0.016	0.083	18.55	–	26	0	–
C21-03	10.24	0.51	0.034	0.001	1.19	0.060	0.020	16.28	0.0112	1	–	–
L8-03	10.20	0.15	0.093	0.010	1.85	0.041	0.001	18.30	0.0059	–	–	0

[a]The first letter L or C denotes, respectively, a laboratory-fabricated or commercial alloy.
L5 is a model austenitic-ferritic alloy that contains globular-shaped ferrite of ≈3 vol.%.
C16 is a Type 316L SS (2.30 wt.% Mo). C21 is a Type 316 SS (Mo 2.08 wt.%).

No good correlation of the degree of IGSCC in the SSRT tests in 289°C water could be obtained with the bulk concentration of Cr, Ni, Si, P, C, N, or O as shown in Fig. 8. However, bulk S concentration provided a good monotonic correlation with percent IGSCC from the SSRT test in 289°C as shown in Fig. 9.

The data in Fig. 9 indicate a strong effect of S at an irradiation level of ≈3 dpa. The four heats of Type 304 and 316 SS containing very low concentrations of S (≤0.002 wt.%) exhibited negligible susceptibility to IGSCC. However, as S content increased to ≥0.003 wt.%, susceptibility increased

drastically. At S contents >0.005 wt.%, the specimens broke in a virtually completely intergranular mode, just as is often observed in IASCC of field components.

The steep increase of susceptibility at >0.003 wt.% in Fig. 9 suggests some kind of critical phenomenon associated with S on or near grain boundaries.

Note that in Fig. 9, only the data for Type 304, 304L, 316, and 316L SSs are shown, and the datum for the ferritic-austenitic steel Heat L5 is not included. The excellent IASCC resistance of the latter heat, which is consistent with good resistance of nonirradiated ferritic-austenitic steels to IGSCC in general, was analyzed in an earlier report.[85] The high resistance of such materials is consistent with the critical role proposed here for S. During melting and cooling of the ingot, most S atoms in this heat are partitioned to delta ferrite in which solubility of S is several times larger than that in austenite in which S solubility is negligible near ≈300°C. Also, ferrite-austenite phase boundaries intersect austenite GBs, therefore, a continuous IG crack path along austenite GBs is difficult to achieve in such duplex steels.

Figure 10 shows the effect of fluence on the degree of IGSCC of five low-S heats, one medium-S heat, and three high-S heats of Type 304 and 316 SS. No low-C heats of Type 304L or 316L SS are included in this figure. For S concentrations ≥0.003 wt.%, the deleterious effect of S in Type 304 and 316 SS increases dramatically as the fluence increases from 0.9 x 10^{21} n cm^{-2} to 2.0 x 10^{21} n cm^{-2}. However, Type 304 and 316 SS heats containing S ≤0.002 wt.% remained resistant to IASCC even at 2.0 x 10^{21} n cm^{-2} (E > 1 MeV) (≈3 dpa).

Figure 11 compares the results of the current investigation with those of other investigations for similar SSRT test conditions, i.e., similar fluence, similar steel type (304, 304L, 316, and 316L), and similar water chemistry. Note that for a DO level of 8–32 ppm the ECP is similar to that in the current tests, i.e., +170 to +220 mV SHE. At ≈3 dpa and S concentrations of ≈0.005 wt.% and higher, the deleterious effect of S is so dominant, leading to virtually complete IGSCC, that it may obscure the effect of other elements. At S concentrations of ≈0.005 wt.% and lower, a beneficial effect of C is manifested significantly. All data in the figure were obtained from steels irradiated with neutrons to a similar fluence level of 1.9 x 10^{21} n cm^{-2} to 2.0 x 10^{21} n cm^{-2} (E > 1 MeV) (≈2.70-2.85 dpa) except for the test reported by Tsukada and Miwa.[79] The high-purity 304L SS heat tested in their investigation contained a high level of S of ≈0.030 wt.%. This heat exhibited as much as 90% IGSCC even at a damage level significantly lower than that of the other investigations.

The deleterious effect of S can be discerned more directly by comparing the IASCC susceptibilities of high– and low–S heats of the same grade that contain otherwise similar elemental compositions, e.g., Heat C12 (S 0.002 wt.%) and Heat C9 (S 0.013 wt.%). As the fluence increased, the susceptibility of Heat C12 remained negligible, whereas the susceptibility of Heat C9 increased drastically; see Fig. 12(A). The relative behavior of Heats C9 and C12 is consistent with the observation reported by Tsukada and Miwa[79] for their HP and HP+S heats; see Fig. 12(B). A similar effect of S was also reported from expanding-tube tests by Kasahara for Type 316LSS,[77] by Jacobs et al. for Type 316L SS;[76] and by Garzarolli et al. for Type 348 SS.[70] The results of these investigations are summarized in Figs. 12(C), (D), and (E), respectively.

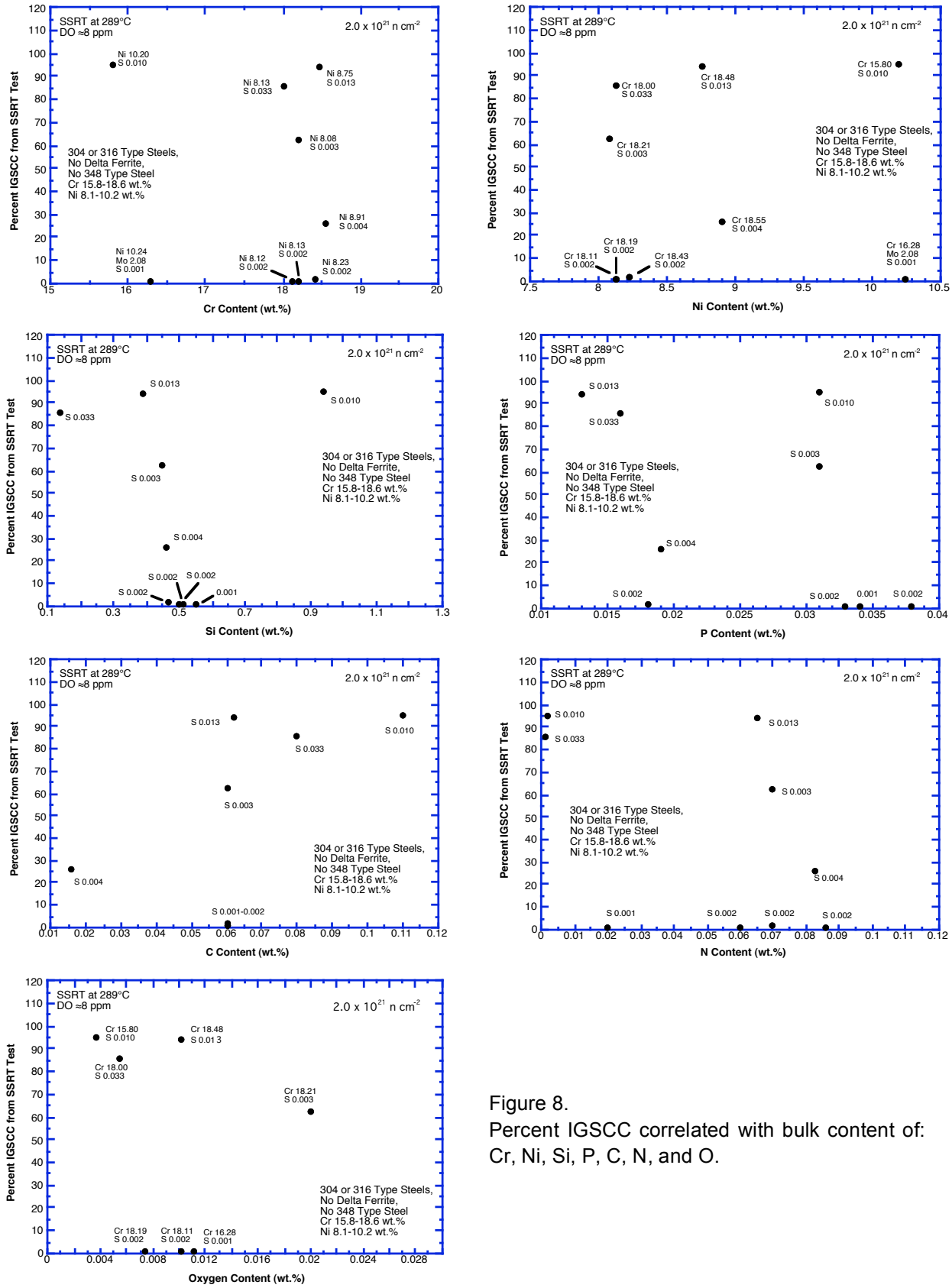

Figure 8.
Percent IGSCC correlated with bulk content of: Cr, Ni, Si, P, C, N, and O.

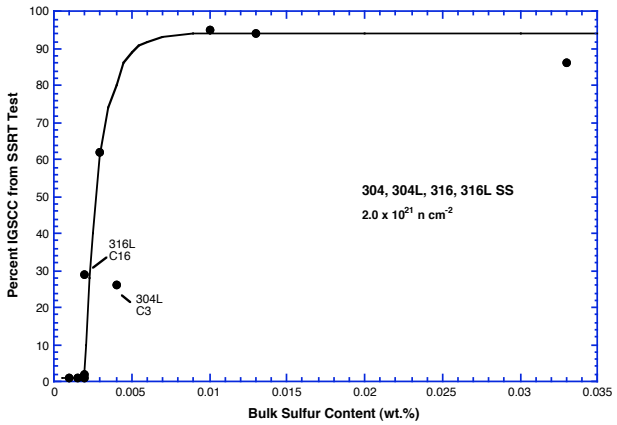

Figure 9.
Percent IGSCC correlated with bulk S content, fluence 2.0 x 10^{21} n cm^{-2} (E > 1 MeV). Only data for Type 304, 304L, 316, and 316L SSs are shown.

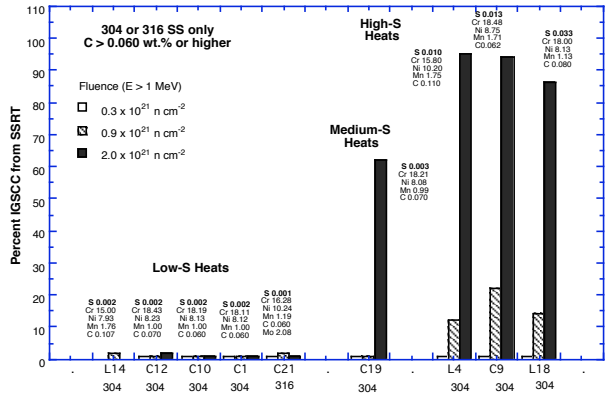

Figure 10.
Percent IGSCC of Types 304 and 316 SS that contain low, medium, and high concentrations of S for three fluence levels.

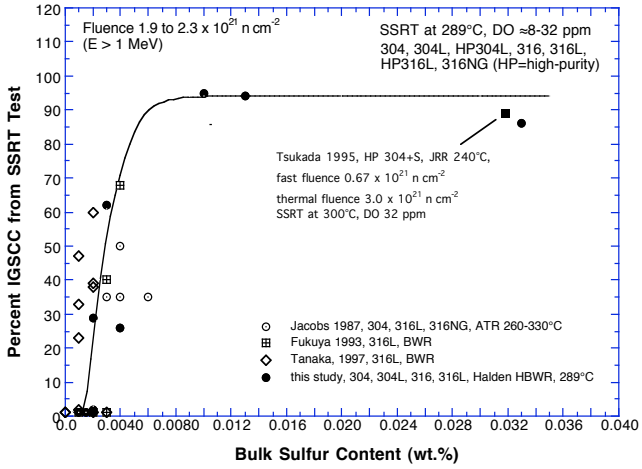

Figure 11.
Percent IGSCC vs. bulk S content for high-C, low-C, and low-C high-purity grades of Types 304 and 316 SS.

The choice of test heats used to obtain the data in Fig. 12(A), (C), (D), and (E) is based on a "binary-like" approach in which S content was varied high or low but the level of other impurity elements were kept similar to those in commercial steels used in reactor components. In contrast, the result in Fig. 12(B) is based on a "single-element" approach in which high-purity (HP) or ultrahigh-purity (UHP) heats are used and the level of a single impurity varied.

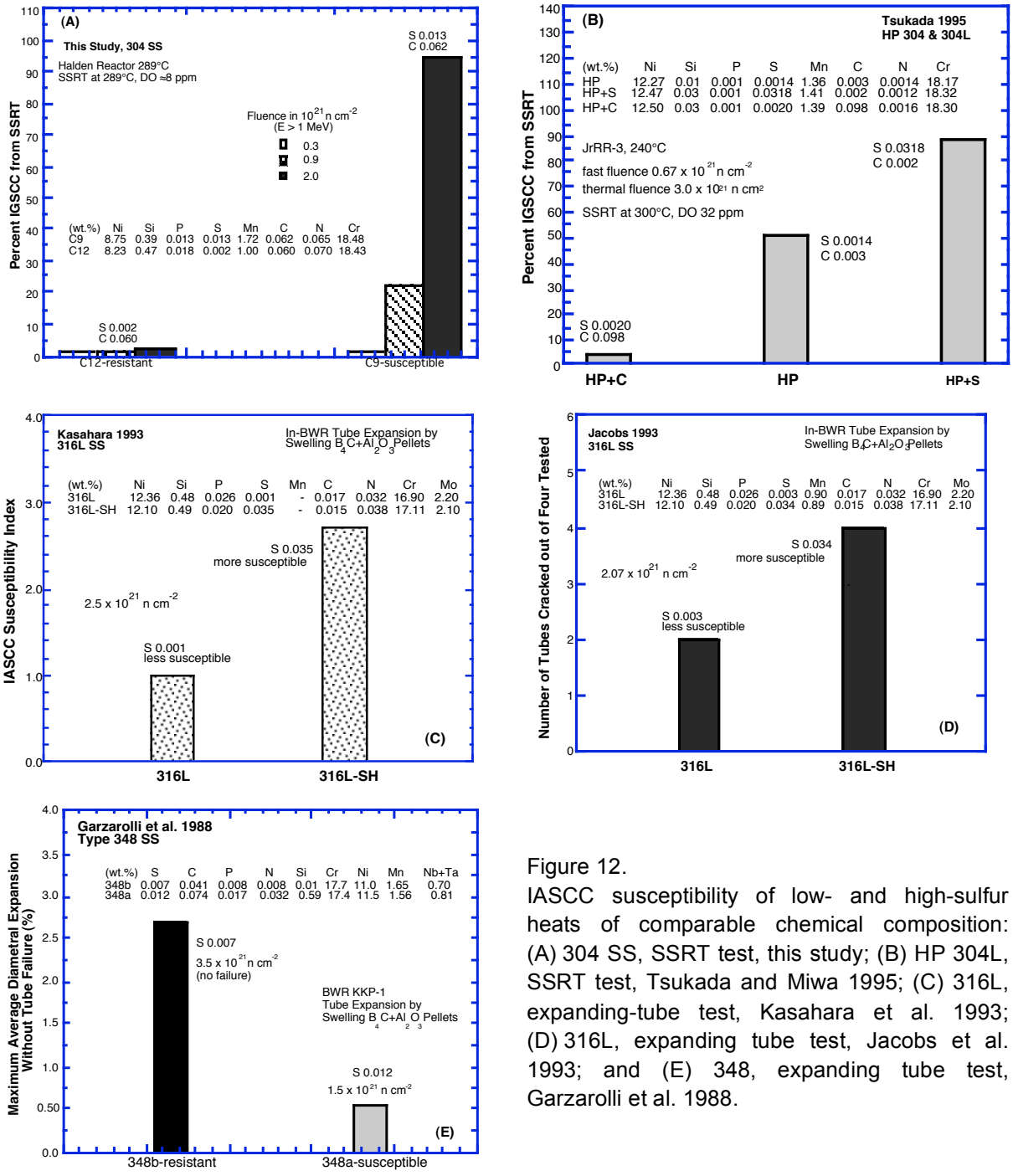

Figure 12.
IASCC susceptibility of low- and high-sulfur heats of comparable chemical composition: (A) 304 SS, SSRT test, this study; (B) HP 304L, SSRT test, Tsukada and Miwa 1995; (C) 316L, expanding-tube test, Kasahara et al. 1993; (D) 316L, expanding tube test, Jacobs et al. 1993; and (E) 348, expanding tube test, Garzarolli et al. 1988.

Note that S content in the HP base heat of Tsukada and Miwa was very low (i.e., 0.0014-0.002 wt.%). In contrast, if the base HP or UHP heat in a "single-element" approach contained a high concentration of S (e.g., >0.004 wt.%), "binary" heats (e.g., HP+Si, HP+C, or HP+P) would have contained similar level of S. Then, it would be difficult to discern the effect of the added single element (e.g., Si, C, or P), because the dominant effect of S would obscure the effects of the other elements.

3.1.4 S Effect in High-Carbon and Low-Carbon Steels

For high-C 304 and 316 SSs, our study indicates that S content of ≤0.002 wt.% provides a good resistance (Fig. 10). However, whether the same is true with low-C 304L, 316L, or HP SSs needs further examination. Type 316 SS Heat C21 that contains 0.001 wt.% S and 0.060 wt.% C was resistant to IASCC (Table 7 and Fig. 10). However, a similar heat (316L Heat C16) containing 0.002 wt.% S and 0.020 wt.% C was susceptible (Table 7 and Fig. 9). This behavior appears to be consistent with the data of Tsukada et al.,[79] i.e., the behavior of Heats HP+C vs. HP shown in Fig. 12(B). They reported that the latter heat with 0.0014 wt.% S and 0.003 wt.% C) was more susceptible than the former heat with 0.0020 wt.% S and 0.098 wt.% C.

Tanaka and coworkers performed SSRT tests after irradiation in a BWR to 1.9 to 2.1 x 10^{21} n cm^{-2} (E > 1 MeV) on 304L and 316L SS heats that contained S in concentrations between 0.000 and 0.003 wt.%.[83] A 304 heat containing 0.002 wt.% S and 0.060 wt.% C was resistant to IASCC at 1.3 x 10^{21} n cm^{-2} (E > 1 MeV), whereas a 304L heat containing 0.002 wt.% S and 0.013 wt.% C was susceptible to IASCC at 2.1 x 10^{21} n cm^{-2} (Fig. 13 top inset). Of the nine 316L heats investigated by Tanaka et al., three exhibited negligible susceptibility to IASCC, whereas the other six exhibited susceptibility. Fukuya et al.[71] reported similar results.

Figures. 13a and b summarize relative IASCC susceptibilities (i.e., percent IGSCC from SSRT test) of low–S heats (S ≤0.002 wt.%) and high–C heats of Type 304 and 316 SS, respectively, relative to those of their low-C counterparts. The trend in the figure indicates that low–S heats (S ≤0.002 wt.%) of 304 and 316 SS are resistant to IASCC. However, low–S heats of 304L and 316L SS are not necessarily resistant.

A similar trend is also evident for the 348 and 348L SSs investigated by Garzarolli and coworkers using the swelling–mandrel technique[66,70,81] (see Fig 13c). In their experiment, the maximum average diametral strain was measured for intact and cracked tubes from the same heat. The consistent behavior observed in the six investigations summarized in Fig. 13 strongly indicates that a high C content suppresses the deleterious effect of S. At S contents of ≤0.005 wt.%, the beneficial effect of C is significant. This effect is a major factor that caused significant data scattering in Fig. 11 at <0.008 wt.% S.

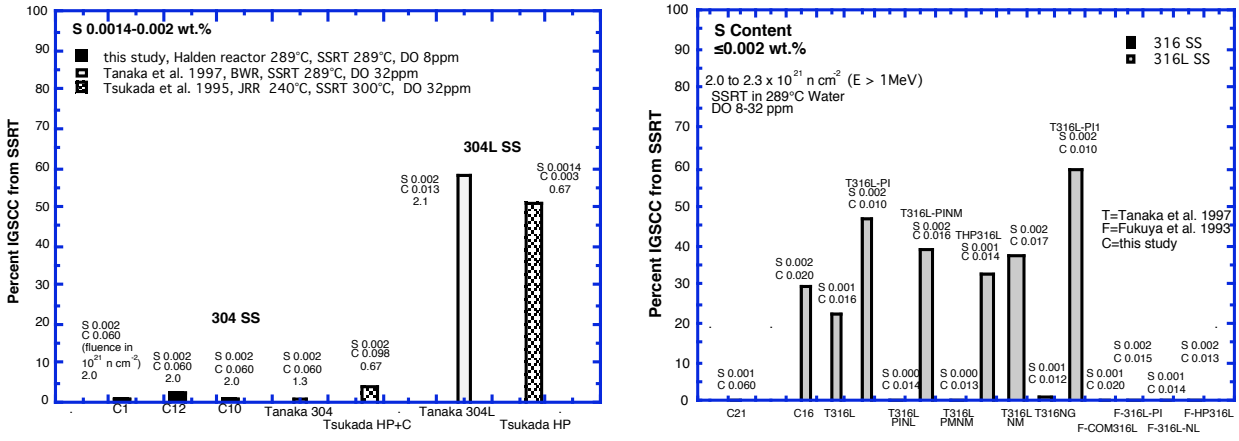

(a) (b)

Figure 13. Percent IGSCC from SSRT test of low-S heats of high– and low–C steels: (a) Type 304 and 304L SSs; (b) 316 and 316L SSs; and (c) 348 and 348L SSs.

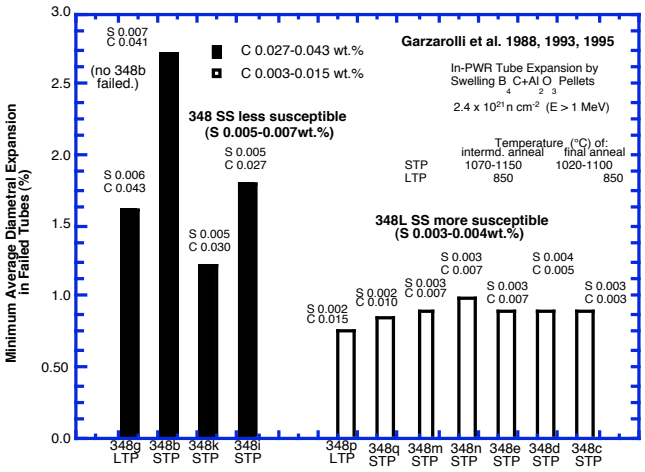

(c)

Figure 13. (Contd.)

3.1.5 Results of Fractography

Figure 14 shows SEM fractographs of the fracture surfaces from the SSRT tests in water at 289°C of the 3-dpa specimens (left column) and the fracture surfaces from the bend tests in 23°C air on the broken SSRT specimen (right column). Several characteristics are observed:

(a) Intergranular fracture surfaces produced in high-S heats are covered with corrosion debris. The shape of the debris is spherical, except for the tetrahedral debris in 304 SS Heat C9.

(b) Little corrosion debris occurs on ductile or transgranular (TG) fracture surfaces.

(c) The width of most grain boundaries separated in 289°C water is very narrow. Grain-boundary separation from bend fracture in 23°C air is wider.

(d) Significant grain encirclement (completely separated loose grains as in sand) is visible in some specimens tested in 289°C water (e.g., C19), but not in samples fractured in 23°C air.

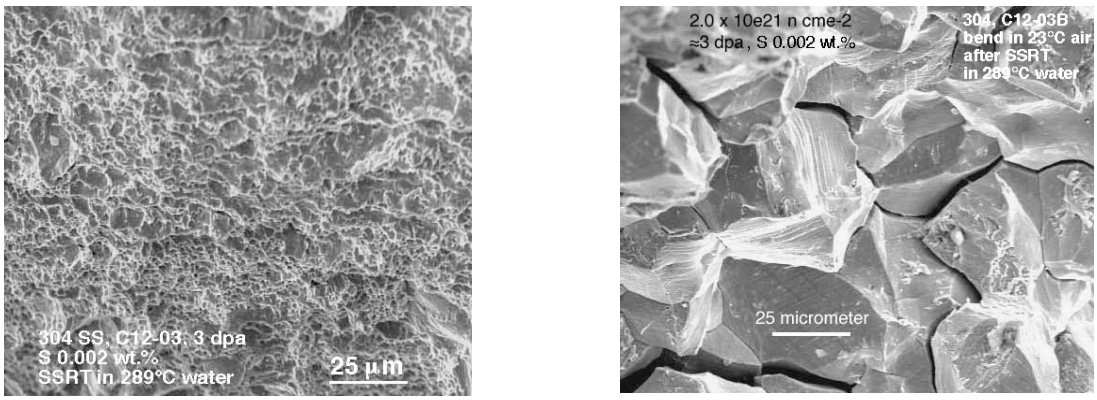

Figure 14. Fracture surface morphology produced during SSRT test in 289°C water (left) and during bending in 23°C air after SSRT test in 289°C water (right). Rows from top to bottom are: Type 304 SS Heat C12, 304 SS C9, 304 SS C19, 304 SS C10, 304 SS L18, and 304 SS C1.

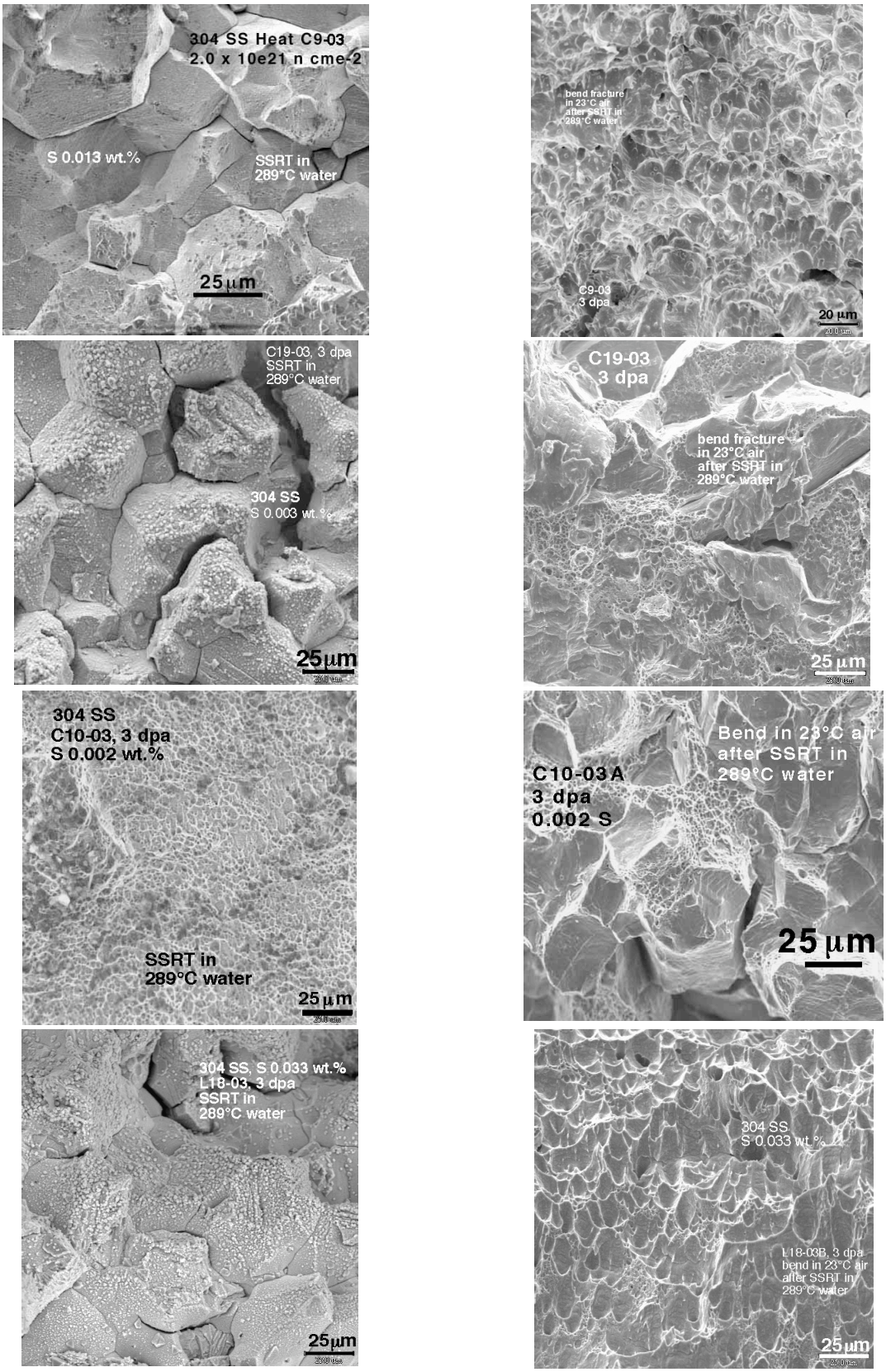

Figure 14. (Continued).

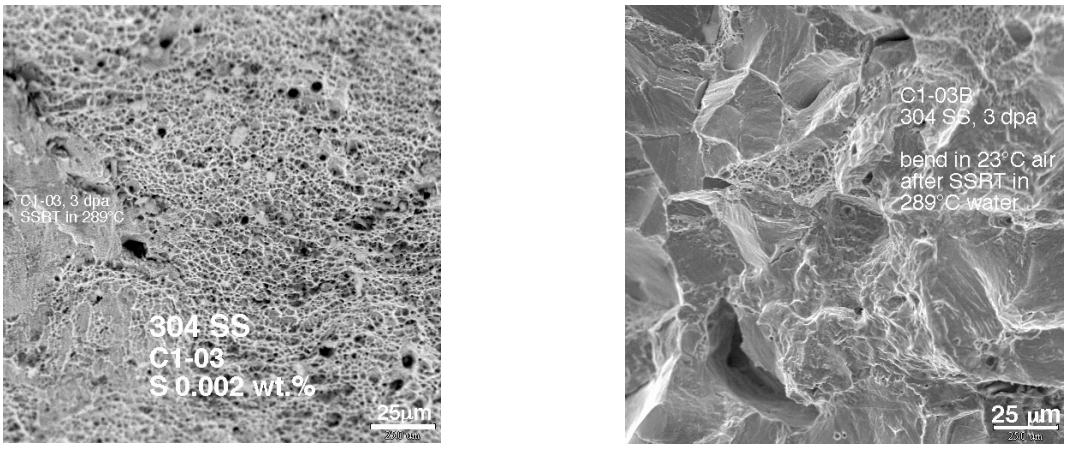

Figure 14. (Continued).

(e) Local regions of ductile dimple occur in the middle of the IG-fracture area in specimens tested in 23°C air, e.g., C10-03A. This was observed in specimens tested in 289°C water.

(f) The IG fracture surface produced in 23°C air shows more deformation steps than IG fracture surfaces produced in 289°C water.

3.1.6 Grain-Boundary Segregation of S and C

The GB segregation of S and C in neutron absorber tubes fabricated from two heats of 304 SS and irradiated to 2.0 x 10^{21} n cm^{-2} (E > 1 MeV) (≈3 dpa) in a commercial BWR was analyzed by AES. Unfortunately, the chemical composition of the tubes or the 304 SS heats could not be documented. The results of the analysis are shown in Fig. 15. In the top-left figure, Auger electron peak heights of S obtained from four ductile fracture surfaces are compared with their counterparts from twelve IG fracture surfaces in Tube A-1 (from 304 SS Heat A). Similar results obtained from the same specimen are also shown for C in the top-right inset. The results show that S and C segregated significantly to GBs (i.e., IG fracture surfaces). Results of automated Ar-ion sputtering and depth-profile analysis, shown in the bottom figure, confirm GB segregation of S and C for Tube A-1 and S segregation for Tube B (from Heat B).

However, the analysis cannot identify whether the GB segregation of S occurred via a thermal process (during fabrication), irradiation-induced process, or both. The latter, radiation–induced segregation (RIS) of S, needs further investigation.

Thermal segregation of S to GBs has been reported by Andresen and Briant for ultra-high-purity (UHP) austenitic SS doped with S.[86] They concluded that the deleterious effect of S plays an important role in producing an IG crack path in sensitized nonirradiated steels. Because S atoms are thermally segregated on GBs, more S ions are released into water from a GB than from a grain matrix. Thus, the role of S was essentially viewed in their study as accelerating corrosive attack (i.e., dissolution of GB metal) of Cr-depleted grain boundaries via release of S ions into crack tip water. According to this model, as long as GBs are significantly depleted of Cr, an IG path would be predicted even in a steel that is free of S.

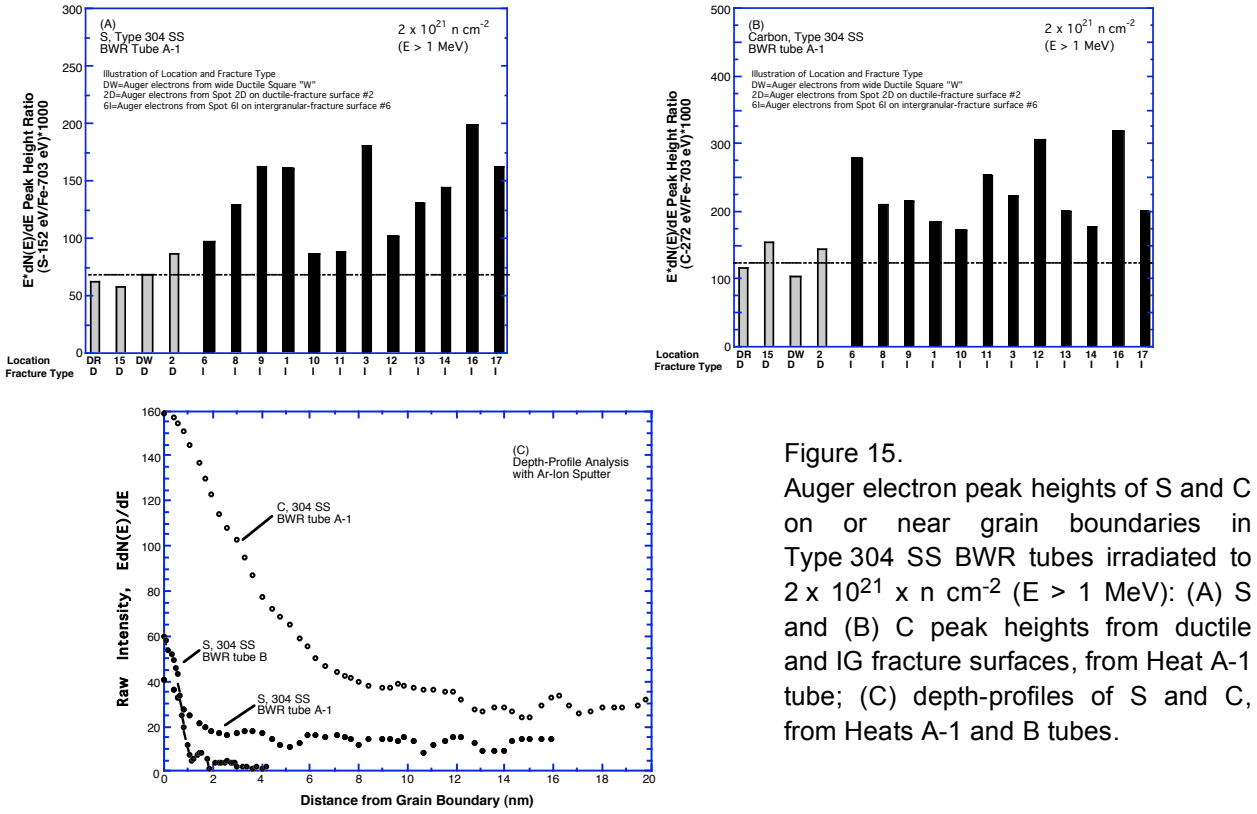

Figure 15.
Auger electron peak heights of S and C on or near grain boundaries in Type 304 SS BWR tubes irradiated to 2 x 10^{21} x n cm^{-2} (E > 1 MeV): (A) S and (B) C peak heights from ductile and IG fracture surfaces, from Heat A-1 tube; (C) depth-profiles of S and C, from Heats A-1 and B tubes.

Such a model of the S effect does not appear to work well in explaining the IASCC susceptibility of irradiated steels. One difficulty is how to explain the observation that IASCC susceptibility becomes negligible when S concentration is extremely low even though the Cr depletion may be significant. Note that significant GB Cr depletion occurs in 304 SSs by the time the damage level reaches ≈3 dpa. The other difficulty is how to explain the trend that the S effect is strongly influenced by fluence at >0.003 wt.% S (Figs. 9–11).

3.2 Crack Growth Rate Test of Austenitic Stainless Steels Irradiated in the Halden Reactor (E. E. Gruber and O. K. Chopra)

3.2.1 Introduction

Austenitic SSs are used extensively as structural alloys in reactor pressure vessel internal components because of their high strength, ductility, and fracture toughness. However, exposure to neutron irradiation changes the microstructure and degrades the fracture properties of these steels. Irradiation leads to a significant increase in yield strength and reduction in ductility and fracture resistance of austenitic SSs.[87–90] Radiation can exacerbate the corrosion fatigue and stress corrosion cracking (SCC) of SSs[87,91,92] by affecting the material microchemistry, e.g., radiation–induced segregation; material microstructure, e.g., radiation hardening; and water chemistry, e.g., radiolysis.

The factors that influence SCC susceptibility of materials include neutron fluence, cold work, corrosion potential, water purity, temperature, and loading. The effects of neutron fluence on IASCC of austenitic SSs have been investigated for boiling water reactor (BWR) control blade sheaths[93,94] and laboratory tests on BWR–irradiated material;[91,95–97] the extent of intergranular SCC increases with

fluence. Although a threshold fluence level of 5×10^{20} n cm^{-2} (E >1 MeV) has been reported for austenitic SSs in the BWR environment, experimental data show an increase in intergranular cracking above a fluence of $\approx 2 \times 10^{20}$ n cm^{-2} (E >1 MeV) (≈0.3 dpa). The results also show the beneficial effect of reducing the corrosion potential of the environment.[98,99] However, low corrosion potential does not provide immunity to IASCC, e.g., intergranular SCC has been observed in cold–worked, irradiated, SS baffle bolts in pressurized water reactors (PWRs). The threshold fluence for IASCC is higher under low potential conditions such as hydrogen water chemistry (HWC) in BWRs or primary water chemistry in PWRs.[100]

This report presents experimental data on crack growth rates (CGRs) of Types 304 and 316 SS irradiated up to 2.0×10^{21} n cm^{-2} (E > 1 MeV) at ≈288°C. The irradiations were carried out in a He environment in the Halden boiling heavy water reactor. Crack growth tests were conducted under cyclic loading with long rise times or constant load in normal water chemistry (NWC) and HWC BWR environments at 288°C.

3.2.2 Experimental

Crack growth tests were performed at ≈289°C on 1/4–T compact tension (CT) specimens in simulated BWR environments; the configuration of the specimens is shown in Fig. 16. Crack extensions were determined by DC potential measurements.

The facility for conducting the tests is designed for in–cell testing, with the hydraulic actuator, test load train, autoclave, and furnace mounted on top of a portable wheeled cart that can be easily rolled into the cell. A detailed description of the facility is presented elsewhere.[101]

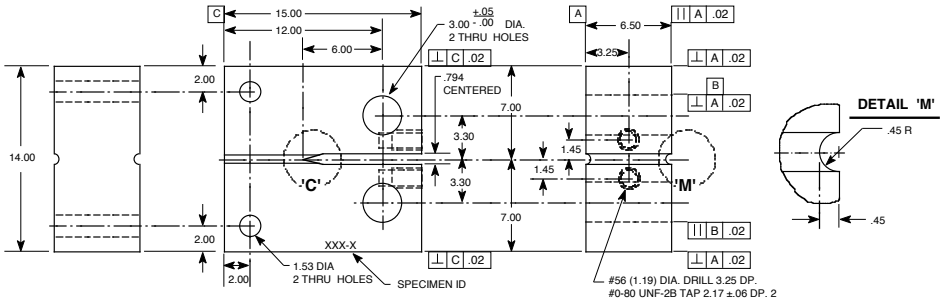

Figure 16. Configuration of compact–tension specimen for this study (dimensions in mm)

The BWR environments comprise high–purity–deionized water that contains either ≈300 ppb or <30 ppb DO resulting in electrochemical potentials (ECPs) for SS that range from 160 to -500 mV. Deionized water is prepared by passing purified water through a set of filters that comprise a carbon filter, an Organex–Q filter, two ion exchangers, and a 0.2–mm capsule filter. The DO level in water is established by bubbling N_2 that contains ≈1% O_2 through the deionized water. The DO level is reduced to <30 ppb by bubbling N_2 through the water. The feedwater is stored in a 135–L SS tank. The cover gas of the feedwater tank is N_2 plus 1% O_2 for the high–DO environment and either pure N_2 or N_2 plus 5% H_2 for the low–DO environment. Water samples are taken periodically to measure pH, resistivity, and DO concentration in the feedwater.

The feedwater is circulated from the storage tank through a high–pressure pump, regenerative heat exchanger, autoclave preheater, test autoclave, ECP cell preheater, ECP cell, regenerative heat exchanger, Mity Mite™ back-pressure regulator, an ion–exchange cartridge, a 0.2–micron filter, a demineralizer

resin bed, another 0.2–micron filter, and then returned to the storage tank. A schematic diagram of the recirculating water system is shown in Fig. 17. Water is circulated at low flow rates, e.g., 10–15 mL/min.

Water samples are taken periodically (from ports 12 or 19 in Fig. 17) to measure the resistivity and DO concentration in the effluent. Also, note that the ECPs of a Pt electrode and SS sample are monitored continuously during the CGR tests downstream from the autoclave. Under the steady state chemistry conditions being studied, the ECP of the SS sample should be representative of the ECP of the actual test specimen.

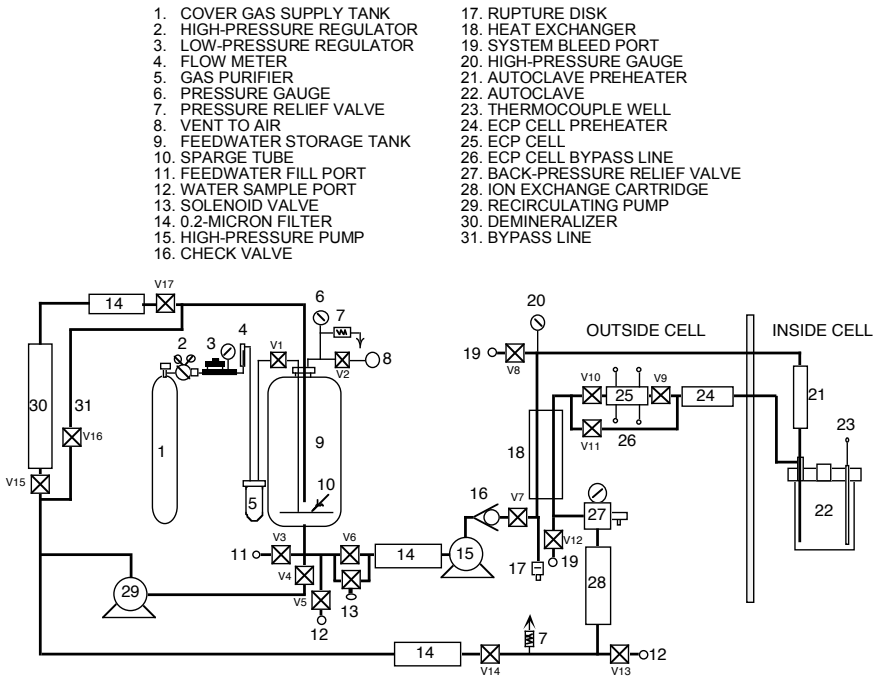

Figure 17. Schematic diagram of recirculating water system

Table 9. Composition (wt.%) of model austenitic stainless steels irradiated in the Halden reactor

ID[a]	Heat ID	Analysis	Ni	Si	P	S	Mn	C	N	Cr	Mo	O[b]
	Type 304 SS											
C3	PNL-C-6	Vendor	8.91	0.46	0.019	0.004	1.81	0.016	0.083	18.55	–	–
		ANL	9.10	0.45	0.020	0.003	1.86	0.024	0.074	18.93	–	144
	Type 316 SS											
C16	PNL–SS–14	Vendor	12.90	0.38	0.014	0.002	1.66	0.020	0.011	16.92	–	–
		ANL	12.32	0.42	0.026	0.003	1.65	0.029	0.011	16.91	2.18	157

[a]First letters "C" denotes commercial heat.
[b]In wppm.

Table 10. Tensile properties of irradiated austenitic stainless steels at 288°C

			Fluence (E > 1 MeV)			
	Nonirradiated		0.9×10^{21} n cm^{-2}		2.0×10^{21} n cm^{-2}	
Steel Type (Heat)	Yield (MPa)	Ultimate (MPa)	Yield (MPa)	Ultimate (MPa)	Yield (MPa)	Ultimate (MPa)
304 SS (C3)	(154)[a]	(433)[a]	632	668	796	826
316 SS (C16)	(189)[a]	(483)[a]	562	618	766	803

[a]Estimated value.

The CGR tests were performed in accordance with ASTM E–647 "Standard Test Method for Measurement of Fatigue Crack Growth Rates" and ASTM E–1681 "Standard Test Method for Determining a Threshold Stress Intensity Factor for Environment–Assisted Cracking of Metallic Materials under Constant Load." The composition of the SSs is presented in Table 9 and the tensile yield and ultimate stresses for the steels irradiated to two fluence levels and in the nonirradiated condition[102,103] are given in Table 10.

All specimens were fatigue precracked at load ratio R = 0.2, ≈1 Hz frequency, and maximum stress intensity factor K_{max} ≈15 MPa $m^{1/2}$. After ≈0.5–mm extension, R was increased incrementally to 0.7, and the loading waveform changed to a slow/fast sawtooth with rise times of 30–1000 s. Constant–load tests were conducted with the trapezoidal waveform, R = 0.7, 1– or 2–h hold period at peak, and either 4– or 24–s unload/reload period. In all tests, K_{max} was maintained approximately constant by periodic load shedding. After the test, the final crack size was marked by fatigue cycling at room temperature. The specimen was then fractured, and the fracture surface of both halves of the specimen was photographed with a telephoto lens through the cell window. The final crack length was measured from the photograph by the 9/8 averaging technique.

To ensure that the experimental data obtained from differing specimen geometry, thickness, and loading conditions can be compared with each other and applied to reactor components, the CGR data were validated in accordance with the specimen size criteria of ASTM E–1681 and E–647. These criteria require that the plastic zone at the tip of a fatigue crack be small relative to the specimen geometry. For constant–load tests,

$$B_{eff} \text{ and } (W-a) \geq 2.5\,(K/\sigma_{ys})^2 \tag{22}$$

and for cyclic loading,

$$(W-a) \geq (4/\pi)\,(K/\sigma_{ys})^2, \tag{23}$$

where the effective specimen thickness B_{eff} is expressed in terms of the specimen thickness B and net specimen thickness B_N, by the relationship $B_{eff} = (B\,B_N)^{0.5}$; W is the specimen width; a is the crack length; K is the applied stress intensity factor; and σ_{ys} is the yield stress of the material. In high–temperature water, because the primary mechanism for crack growth under cyclic loads with long rise times is not mechanical fatigue, Eq. 22 is probably the more appropriate requirement and was used in the present study; but, Eq. 23 may give acceptable results. For high–strain–hardening materials, i.e., materials with ultimate–to–yield–stress ratio ≥1.3, the K/size criteria are generally conservative. Violating them by a small amount, e.g., 20–30% in K, is probably acceptable, but violating by 50–100% is very likely to cause problems.

The K/size criteria were developed for materials that show work hardening and, therefore, may not be valid for materials irradiated to fluence levels where, on a local level, they do not strain harden. This lack of strain hardening or strain softening is most dramatic when dislocation channeling occurs but may also occur at lower fluences. For moderate to highly irradiated material, it has been suggested that an effective yield stress, defined as the average of the nonirradiated and irradiated yield stresses, be used.[104] This discounts the irradiation–induced increase in yield stress by a factor of 2. This modification of the K size criteria has been used in the current analysis.

3.2.3 Crack Growth Rates of Irradiated Stainless Steels in BWR Environments

Crack growth tests at 289°C have been completed on 1/4–T CT specimens of Type 304 SS (Heat C3) irradiated to 0.9 and 2.0×10^{21} n·cm^{-2} and Type 316 SS (Heat C16) irradiated to 2.0×10^{21} n·cm^{-2}. The results are given in Tables 11–13. The ECPs of a Pt electrode and SS electrode were monitored continuously during each test, whereas the water DO level and conductivity were measured periodically. Some significant results from these tests are presented below.

All tests were started in high–purity water that contained 250–300 ppb DO (i.e., NWC BWR environment). After data were obtained for high–DO water, the DO level in the feedwater was decreased to <30 ppb by sparging the feedwater with pure N_2 and, in some cases, followed by sparging with N_2 + 5% H_2 (to simulate HWC). Because of the very low water flow rates, it took several days for the environmental conditions to stabilize. Changes in crack length and ECP of the Pt and SS electrodes during these transient periods are shown in Fig. 18 for specimen C3–B. The changes in steel ECP were slower than in the Pt ECP. For example, although the Pt ECP decreased below –400 mV (SHE) within 40 h, it took more than 150 h for the steel ECP to decrease below –400 mV.

Table 11. Crack growth results for Specimen C3–B of Type 304 stainless steel[a] in high–purity water at 289°C

Test	Test Time,	ECP[b] mV (SHE)		O_2 Conc.,[b]	Load	Rise Time,	Down Time,	Hold Time,	K_{max}	ΔK,	Growth Rate,	Allowed K_{max}	Margin in K_{max}
Period	h	Pt	Steel	ppb	Ratio	s	s	s	MPa·m$^{1/2}$		m/s	MPa m$^{1/2}$	%
1	28	230	154	300	0.20	0.5	0.5	0	19.1	15.31	6.83E-08	18.4	3.8
2	172	239	189	300	0.51	60	2	0	19.0	9.29	1.75E-10	18.3	3.4
3	287	233	187	300	0.70	300	2	0	19.8	5.94	6.38E-10	18.0	9.7
4	335	235	191	300	1.00[c]	2	2	7200	20.1	0	1.06E-09	17.7	13.6
5	376	238	195	300	1.00[c]	2	2	7200	22.1	0	1.04E-09	17.4	27.1
6	624	-475	–595	≈10	1.00[c]	2	2	7200	22.3	0	4.02E-11	17.2	29.7
7	696	-482	–607	≈10	0.70	300	2	0	22.1	6.63	8.56E-11	17.1	29.1
8	935	-495	–614	≈10	1.00[c]	2	2	3600	22.7	0	6.42E-12	17.1	32.4
8	935	-495	–614	≈10	1.00[c]	2	2	3600	22.7	0	6.42E-12	17.1	32.4
9	1031	-499	–609	≈10	0.70	300	2	0	22.5	6.76	3.37E-11	17.1	31.8
10a	1127	-495	–613	≈10	0.70	1000	2	0	22.2	6.66	negligible	17.1	29.9
10b	1271	-507	–620	≈10	0.70	1000	2	0	23.0	6.91	1.20E-11	17.1	34.9
11	1295	-507	–624	≈10	0.70	30	2	0	22.9	6.86	5.17E-11	17.1	34.0
12	1343	-498	–617	≈10	0.70	300	2	0	23.1	6.93	1.55E-11	17.1	35.5
14	1608	248	151	250	0.70	1000	2	0	24.2	7.25	5.93E-10	16.7	45.1
15	1655	244	155	250	1.00[c]	2	2	3600	24.4	0	8.70E-10	16.4	49.2

[a] Heat C3, irradiated to 0.9×10^{21} n cm^{-2}.
[b] Represents values in the effluent. Conductivity was 0.07 and 0.3–0.45 μS/cm in feedwater and effluent, respectively. Feedwater pH at room temperature was 6.5.
[c] Constant load test with periodic unload to R = 0.7 every 1 or 2 h; 4 s unload/reload period.

Under cyclic loading, the CGR (m/s) can be expressed as the superposition of the rate in air (i.e., mechanical fatigue) and the rates due to corrosion fatigue and SCC, given as

$$\dot{a}_{env} = \dot{a}_{air} + \dot{a}_{CF} + \dot{a}_{SCC}. \quad (24)$$

The results indicate that environmental enhancement of CGRs does not occur from the start of the test. Under more rapid cyclic loading, the crack growth is dominated by mechanical fatigue. The CGRs during precracking and initial periods of cyclic loading were primarily due to mechanical fatigue. For the present tests on irradiated SSs, environmental enhancement typically was observed under loading

conditions that would lead to CGRs between 10^{-10} and 10^{-9} m/s in air. For K_{max} values of 15–18 MPa $m^{1/2}$, these values correspond to a load ratio R ≥ 0.5 and rise time ≥ 30 s.

Table 12. Crack growth results for Specimen C3–C of Type 304 SS[a] in high–purity water at 289°C

Test Period	Test Time, h	ECP[b] mV (SHE) Pt	ECP[b] mV (SHE) Steel	O_2 Conc.,[b] ppb	Load Ratio	Rise Time, s	Down Time, s	Hold Time, s	K_{max} MPa $m^{1/2}$	ΔK, MPa $m^{1/2}$	Growth Rate, m/s	Allowed K_{max} MPa $m^{1/2}$	Margin in K_{max} %
1	46	241	164	300	0.26	2	2	0	17.9	13.2	2.00E-08	22.4	-20.2
2	71	223	155	300	0.53	30	2	0	18.4	8.65	2.22E-09	22.1	-16.9
3	99	235	167	300	0.70	300	2	0	18.8	5.64	1.73E-09	21.8	-13.9
4	142	232	164	300	0.69	1000	2	0	19.2	5.96	1.25E-10	21.4	-10.3
5	191	233	164	300	1.00[c]	2	2	3600	19.4	0	6.83E-10	21.1	-8.1
6	311	-450	7	100	1.00[c]	2	2	3600	23.7	0	5.07E-10	20.5	15.5
7	560	-547	-294	10	1.00[c]	2	2	3600	27.5	0	6.91E-10	19.1	44.2
8	706	-551	-502	10	1.00[c]	2	2	3600	34.7	0	2.04E-09	16.4	111.4
9	724	-557	-457	10	1.00[c]	2	2	3600	37.0	0	3.70E-09	15.8	133.9

[a]Heat C3, irradiated to 2.0 x 10^{21} n cm^{-2}.
[b]Represents values in the effluent.
Conductivity was 0.07 and 0.3–0.45 μS/cm in feedwater and effluent, respectively. Feedwater pH at room temperature was 6.5.
[c]Constant load test with periodic unload to R = 0.7 every 1 or 2 h; 4 s unload/reload period.

Table 13. Crack growth results for Specimen C16–B of Type 316 SS[a] in high–purity water at 289°C

Test Period	Test Time, h	ECP[b] mV (SHE) Pt	ECP[b] mV (SHE) Steel	O_2 Conc.,[b] ppb	Load Ratio	Rise Time, s	Down Time, s	Hold Time, s	K_{max} MPa $m^{1/2}$	ΔK, MPa $m^{1/2}$	Growth Rate, m/s	Allowed K_{max} MPa $m^{1/2}$	Margin in K_{max} %
1	94	224	148	250	0.56	12	2	0	14.6	6.4	4.94E-10	22.2	-34.8
2	132	226	147	250	0.73	30	2	0	14.8	4.0	8.65E-10	22.0	-33.1
3	173	228	151	250	0.71	300	2	0	15.0	4.4	8.16E-10	21.8	-31.2
4	198	224	153	250	0.70	1000	12	0	15.0	4.5	7.33E-10	21.7	-30.6
5	265	162	117	250	1.00[c]	12	12	3600	15.2	0	4.62E-10	21.4	-28.9
6	410	-547	-298	<30	1.00[c]	12	12	3600	15.2	0	1.90E-11	21.3	-28.4
7	504	-562	-410	<30	0.70	1000	12	0	15.2	4.54	2.76E-11	21.3	-28.9
8	527	-560	-449	<30	0.73	30	2	0	15.2	4.10	6.07E-11	21.3	-28.7
9	552	-557	-502	<30	0.70	30	2	0	17.3	5.18	2.51E-10	21.2	-18.4
10	600	-554	-545	<30	0.69	1000	12	0	17.2	5.34	3.59E-11	21.2	-18.5
11	672	-557	-554	<30	1.00[c]	12	12	3600	17.3	0	1.73E-11	21.1	-18.3
12	792	-438	-597	<30	1.00[c]	12	12	3600	19.7	0	4.11E-11	21.1	-6.8
13	866	219	139	250	1.00[c]	12	12	3600	19.6	0	7.14E-10	21.0	-6.5
14	871	224	148	250	1.00[c]	12	12	3600	21.9	0	1.10E-09	20.9	4.6
15	888	224	148	250	1.00[d]	0	0	–	21.9	–	5.27E-10	20.9	4.9

[a]Heat C16, irradiated to 2.0 x 10^{21} n cm^{-2}.
[b]Represents values in the effluent. Effluent conductivity was ≈0.45 μS/cm and DO was ≈250 ppb during high–DO test and <40 ppb during low–DO test. Feedwater conductivity was 0.07 μS/cm and pH at room temperature was 6.5.
[c]Constant load test with periodic unload/reload to R = 0.7 every 1 h.
[d]Constant displacement test.

The crack–length–vs.–time plots for specimens C3–B, C16–B, and C3–C are shown in Figs. 19–21. For specimen C3–B, environmental enhancement started at ≈170 h, when R and rise time, respectively, were changed from 0.5 and 60 s to 0.7 and 300 s (Fig. 19). For the new loading condition, although the predicted CGR in air decreased by a factor of ≈15, the rate in water increased by a factor of ≈3. Similarly, for specimen C16–B, enhancement occurred at ≈130 h, when the rise time was increased from 30 to 300 s (Fig. 20). Although the predicted CGR in air decreased by a factor of 10, the rate in water did not change.

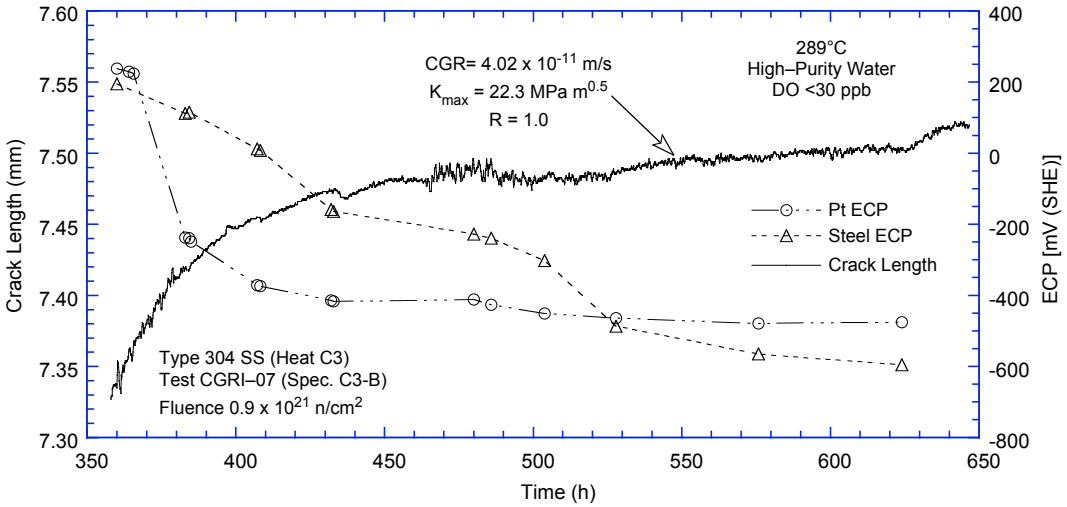

Figure 18. Change in crack length and ECP of Pt and SS electrodes for specimen C3–B after DO level in feedwater was decreased from ≈400 to <30 ppb

Tables 11–13 list the allowed K_{max} for the various test periods based on Eq. 22 and the deviation in the experimental K_{max} from the allowed value. For specimen C16–B, the loading conditions for all test periods satisfy the K/size criterion of Eq. 22 using the proposed effective yield stress for irradiated materials.

For specimen C3–B, during Test Periods 1–4 the experimental K_{max} values were 4–14% higher than the allowable value based on the effective yield stress and 30–50% higher during Periods 5–15. (The loading conditions for all test periods would satisfy the K/size criterion of Eq. 22 if the actual values of yield stress were used.) The crack–length–vs.–time plots in Figs. 19 and 20 show that environmental factors still strongly influenced the CGR at these K levels. For example, the CGRs decreased by a factor of ≈20 when the DO level was decreased from ≈300 to 10 ppb.

For specimen C3–C, the loading conditions meet the criterion of Eq. 22 for Test Periods 1–5 and violate the criterion for Periods 6–9, e.g., deviation in K_{max} is ≈16% for Period 6, ≈44% for Period 7 and

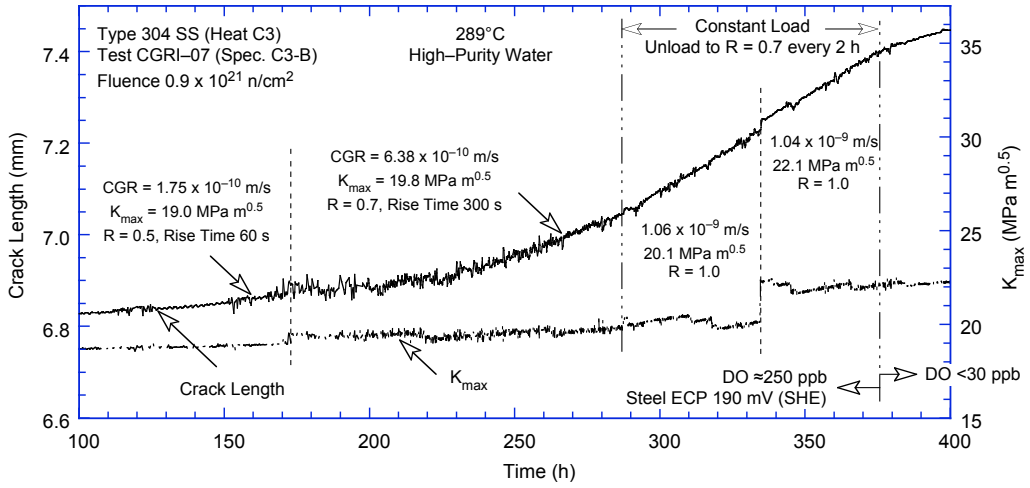

Figure 19. Plots of crack length and K_{max} vs. time for specimen C3–B in high–purity water at 289°C

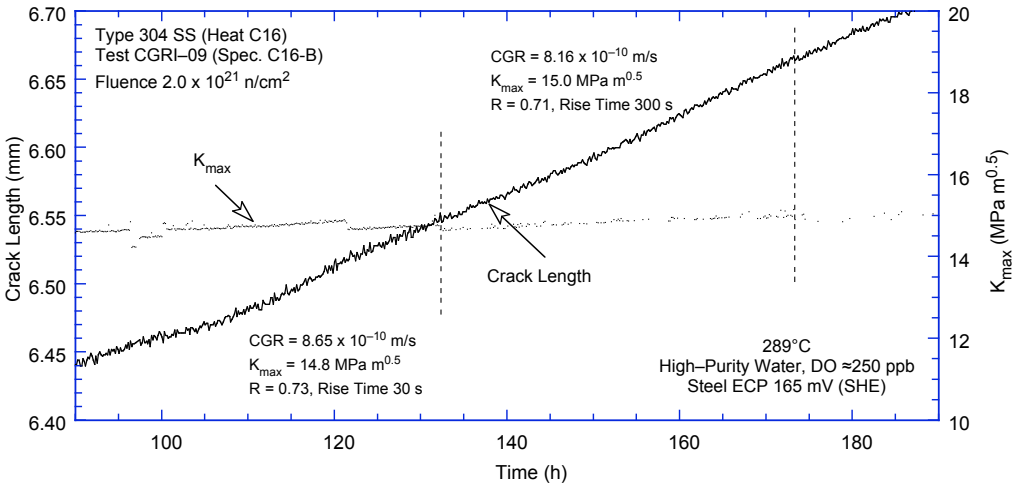

Figure 20. Plots of crack length and K_{max} vs. time for specimen C16–B in high–purity water at 289°C

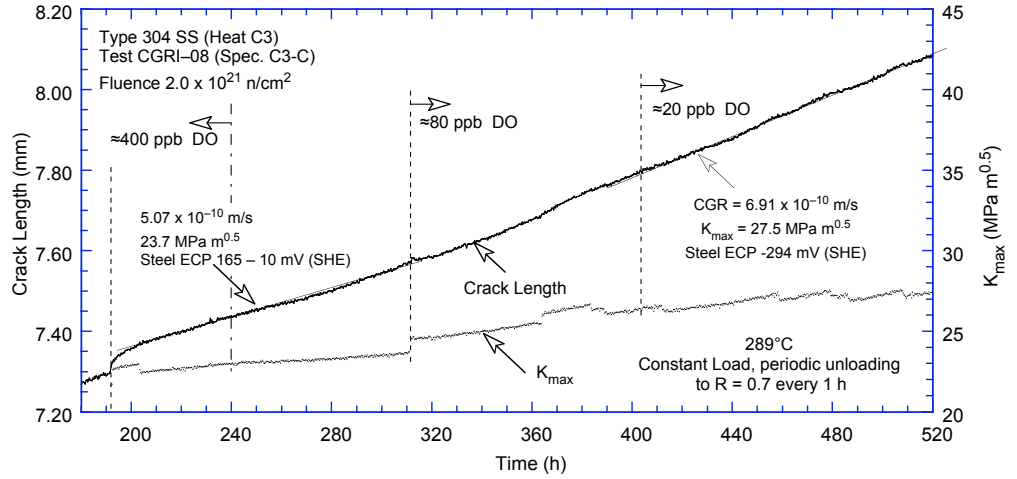

Figure 21. Plots of crack length and K_{max} vs. time for specimen C3–C in high–purity water at 289°C

>100% for Periods 8 and 9. Additional data will be obtained on Type 316 SS Heat C21 irradiated to 0.9 and 2.0 x 10^{21} n·cm^{-2} to validate these results.

For each test, the final crack length was measured from a photograph of the fracture surface (Fig. 22), and the results were used to verify the data obtained from DC potential measurements. The difference in measured crack length and that estimated from the DC potential method, was <5% for Specimens C3–B and C16–B, and ≈40% for Specimen C3–C. The large difference for Specimen C3–C most likely was due to some unbroken ligaments observed on the fracture surface that provided additional conducting paths. For this test, the crack extensions estimated from the DC potential method were scaled proportionately to match the fractographic results.

For cyclic loading, the experimental CGRs for irradiated austenitic SSs in high– and low–DO environments and those predicted in air for the same loading conditions are plotted in Fig. 23. The curves represent the best–fit values for nonirradiated austenitic SSs in high–purity water with either 8 or 0.2 ppm

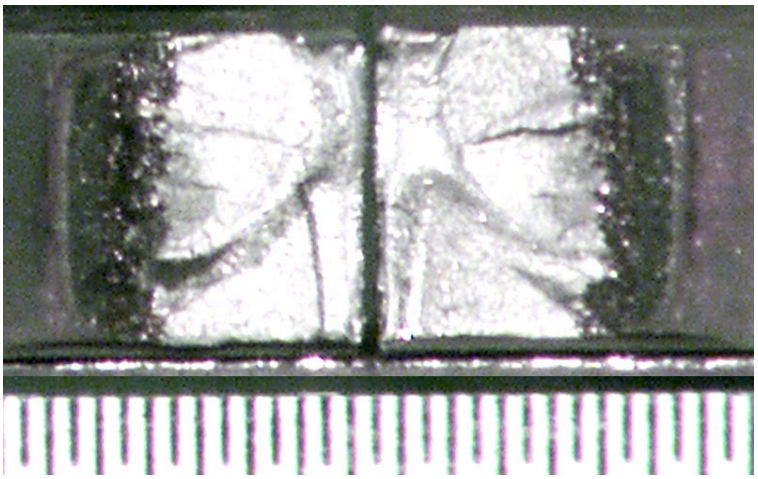

Figure 22. Photomicrograph of fracture surface of specimen C3–B

DO and are included to provide a comparison with the irradiated CGR data.[105] The CGRs in air $\dot{a}_{air}$ (m/s) were determined from the correlations developed by James and Jones.[106]

The results indicate significant enhancement of the CGRs of irradiated steel in high–DO water under cyclic loading with long rise times (Fig. 23a). The CGRs for Type 304 SS irradiated to either 0.9 or 2.0 x 10^{21} n·cm^{-2} (1.35 or 3.0 dpa), and Type 316 SS irradiated to 2.0 x 10^{21} n·cm^{-2} (3.0 dpa) are comparable. In general, the CGRs are slightly higher for the irradiated steels in water with ≈ 300 ppb DO than for nonirradiated austenitic SSs in high–purity water with 8 ppm DO (Fig. 23a).

For cyclic loading, decreasing the DO level has a beneficial effect on CGRs, e.g., decreasing the DO from ≈300 ppb DO to <30 ppb DO results in a factor of 25 decrease in the CGR. The growth rates are slightly lower for the irradiated steels in water with <30 ppb DO than for nonirradiated austenitic SSs in high–purity water with 0.2 ppm DO (Fig. 23b).

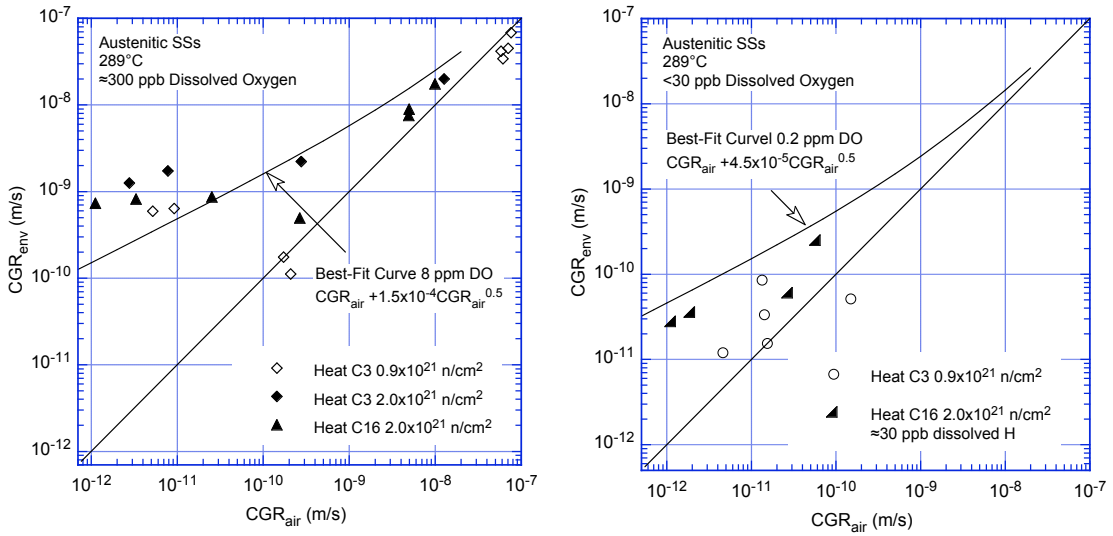

(a) (b)

Figure 23. CGR data for irradiated austenitic SSs under cyclic loading at 289°C in high–purity water with (a) ≈300 ppb and (b) <30 ppb dissolved oxygen.

For an almost constant load (i.e., a trapezoidal waveform), the experimental CGRs for irradiated SSs in high– and low–DO water are plotted in Fig. 24. In high–DO water, the CGRs obtained in the present study of Types 304 and 316 SS irradiated up to 2.0 x 10^{21} n·cm^{-2} (3.0 dpa) are a factor of ≈5 higher than the disposition curve for sensitized SSs in water with 8 ppm DO given in NUREG–0313.[107] The growth rates for the two steels at the same fluence level, as well as those for Type 304 SS irradiated to differing fluence levels, are comparable. The results also indicate a benefit from a low–DO environment. For Heat C3 irradiated to 0.9 x 10^{21} n·cm^{-2} (1.35 dpa) and Heat C16 irradiated to 2.0 x 10^{21} n·cm^{-2} (3.0 dpa) (circles and triangles in Fig. 24), the CGRs decreased more than an order of magnitude when the DO level was decreased from ≈300 to <30 ppb.

No benefit of low–DO environment was observed for Heat C3 irradiated to 2.0 x 10^{21} n·cm^{-2} (3.0 dpa) (open and closed diamonds in Fig. 24). However, the applied K_{max} for the test period in low–DO water was 44% greater than the allowable value based on the K/size criterion in Eq. 22. Additional data are being obtained on Type 304 SS Heat C3 irradiated to 0.3 x 10^{21} n·cm^{-2} (0.45 dpa) and Type 316 SS Heat C21 irradiated to 0.9 and 2.0 x 10^{21} n·cm^{-2} (1.35 and 3.0 dpa), to better establish the effect of decreased DO level on the CGRs of irradiated austenitic SSs.

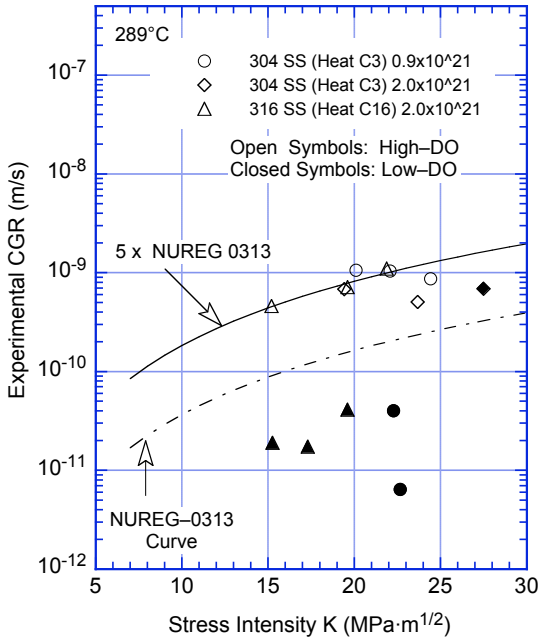

Figure 24.
Crack growth rate under constant load for irradiated austenitic SSs in high–purity water